Stress-Responsive Transcriptomic Signatures in Human iPSC-Derived Microglia Reveal Links to Alzheimer's Disease Risk Genes

Devin Saunders[1], Faraz Sultan[1], Ricardo A. Vialle[1], Nicola A. Kearns[1,2], Bernard Ng[1], Eric M. Clark[1], Himanshu Vyas[1], Sashini De Tissera[1], Jishu Xu[1], David A. Bennett[1,2], Yanling Wang[1,2,] *

1. Rush Alzheimer's Disease Center, Rush University Medical Center, Chicago, IL, 60612, USA
2. Department of Neurological Sciences, Rush University Medical Center, Chicago, IL, 60612, USA

*Correspondence to yanling_wang@rush.edu

Keywords: iPSC-derived Microglia; Cellular Stress Responses; Alzheimer's Disease; Single-Cell RNA Sequencing; CRISPR Interference

Abstract

Cellular stress responses are essential for maintaining homeostasis in the face of environmental or internal challenges. In the central nervous system, microglia serve as key stress sensors and immune responders, shaping neuroinflammatory processes and disease progression. However, the molecular programs engaged by distinct stressors and their impact on microglial viability remain incompletely understood.

In this study, we used human induced pluripotent stem cell-derived microglia-like cells to investigate stress responses to amyloid beta (Aβ), a chronic Alzheimer's disease–related stressor, and lipopolysaccharide (LPS), a classical acute inflammatory stimulus. Using single-cell RNA sequencing, we mapped the transcriptional programs activated by each condition and benchmarked these states against reference microglial datasets from mouse and human brains. In parallel, we performed a pooled CRISPR interference screen targeting Alzheimer's disease-associated microglial genes to identify genetic determinants of microglial survival.

We found that Aβ and LPS elicit partially overlapping but distinct transcriptional responses. Aβ induced more focused and disease-associated gene expression changes, while LPS triggered broad inflammatory activation and stronger cell death signatures. A subset of genes activated by stress overlapped with Alzheimer's disease risk genes and with hits from the survival screen, suggesting that disease-associated microglial genes may contribute to stress adaptation and cellular fitness.

These results demonstrate that iPSC-derived microglia-like cells can recapitulate in vivo–like stress-responsive states and offer a tractable platform to investigate genetic and environmental influences on microglial behavior. Together, our findings reveal transcriptional programs that link stress sensing, survival regulation, and Alzheimer's disease–associated gene networks, providing a foundation for future efforts to enhance microglial resilience in neurodegenerative disease contexts.

Introduction

Stress responses are fundamental cellular programs that maintain homeostasis in the face of internal or external challenges. In the central nervous system, microglia—the brain's resident immune cells—play a key role as stress sensors and responders (1,2). They integrate a wide range of environmental cues, including pathogen exposure, injury, and neurodegenerative insults(3). Disruption of microglial homeostasis by persistent stressors is increasingly recognized as a contributor to disease progression in neurodegenerative conditions such as Alzheimer's disease (AD)(4–7)

Among the stressors implicated in AD, the amyloid-β (Aβ) peptide represents a chronic, disease-relevant signal that may trigger innate immune responses and engage microglia in maladaptive ways. In contrast, lipopolysaccharide (LPS) is a potent exogenous inflammatory stimulus that models acute innate immune activation and systemic inflammation. While both Aβ and LPS are widely used to interrogate microglial responses, the extent to which they elicit shared or distinct molecular, phenotypic, and survival programs in human microglia remains incompletely defined.

To address this, we employed a multi-modal approach using human induced pluripotent stem cell-derived microglia-like cells (iMGLs) exposed to either Aβ or LPS. We performed single-cell RNA sequencing to characterize transcriptional responses and benchmarked iMGL states against human and mouse brain microglia. We further assessed morphological and functional changes associated with stress exposure and leveraged a pooled CRISPR interference (CRISPRi) screen targeting 168 AD-associated genes to identify regulators of microglial survival during differentiation.

Integrating these data, we found that Aβ and LPS induce partially overlapping but distinct stress response programs, with Aβ eliciting a more specific transcriptional signature and LPS driving a broader inflammatory phenotype. Importantly, we identified subsets of stress-responsive genes that overlap with AD risk genes and with survival regulators identified by our CRISPRi screen, providing

66 mechanistic insight into how microglia respond to distinct stressors. These findings underscore the
67 utility of iPSC-derived microglia as a disease-relevant model for studying microglial stress response
68 and reveal new candidate pathways for promoting microglial resilience in neurodegenerative disease
69 contexts.

70 Methods

71 Maintenance of iPSCs

72 All stem cell work was performed in compliance with the Rush University Medical Center IBC
73 committee. Cells were incubated at 37 °C, 5% CO2 under normoxic conditions during all experiments
74 and stimulations unless otherwise specified. Two iPSC lines (BR9 and BR28) were previously
75 generated from white blood cells collected from participants in the Rush Memory and Aging Project
76 (MAP) by the New York Stem Cell Foundation and banked in house (8,9), The dCas9-KRAB iPSC
77 iPSC line was developed at the Allen Institute for Cell Science (allencell.org/cell-catalog) and
78 available through the Coriell Institute for Medical Research (AICS-0090-391). This Allen Cell line was
79 derived from the WTC parental line released by the Conklin Laboratory at the J. David Gladstone
80 Institute. iPSCs were maintained on hESC-qualified Matrigel (Fisher, 8774552) coated 10cm dishes
81 in mTESR Plus (StemCell Technologies, 5825) and passaged every 3-4 days with ReLeSR (StemCell
82 Technologies, 5872) according to the manufacturer's protocol.

83 Generation of iPSC-derived microglia like cells (iMGLs)

84 iMGLs were generated according to previously published protocols(10,11) with the following minor
85 adjustments. iPSCs were seeded in hESC-qualified Matrigel-coated plates in mTESR Plus
86 supplemented with Y-27632 ROCK Inhibitor (RI,10mM; Stem Cell Technologies, 72304) and cultured
87 for 24-48 hours. On d0, colonies were switched to iPSC-derived hematopoietic progenitor (iHPC)
88 basal media supplemented with FGF2, BMP4, Activin-A, and LiCl. On d2, cultures were fed with iHPC

89 basal media supplemented with FGF2 and VEGF. On d4, cultures were fed with iHPC basal media
90 supplemented with FGF2, VEGF, TPO, SCF, IL-6, and IL-3. Cultures were given a half media change
91 every two days until d12. On d12, iHPCs were collected, washed, and resuspended in iMGL basal
92 media supplemented with M-CSF, IL-34, and TGFβ-1. Without removing the conditioned media, cells
93 were fed with complete iMGL differentiation media every two days until d30 and expanded as
94 needed. From d30 – d40, cells were fed with iMGL basal media supplemented with M-CSF, IL-34,
95 TGFβ-1, plus maturation factors CD200 and CX3CL1. Media formulations and concentrations can be
96 found in Table S1.

97 **Aβ preparation and labeling**

98 Amyloid-beta ($A\beta_{1-42}$) was reconstituted and aggregated according to Labeling Amyloid Beta with
99 pHrodo Red protocol from Fujifilm Cellular Dynamics Inc. All reagents required to reconstitute Aβ
100 were provided in the aggregation kit (rPeptide, A-1170-2). Briefly, lyophilized Aβ was reconstituted in
101 250 uL 10 mM NaOH and transferred to a 1.5 mL microcentrifuge tube. 250 uL of HPLC water was
102 added, followed by 56 uL 10x TBS (pH 7.4). The reconstituted AB was allowed to aggregate in an
103 incubator overnight under normoxic conditions. After overnight incubation, the aggregates were
104 collected by centrifugation at 16,000 x g for 1 min at room temperature. Supernatant was removed
105 and aggregates were washed with 200 µL fresh 0.1 M NaHCO3 (Sigma, 144-55-8) in water. 1 mg of
106 pHrodo Red, Succinimidyl Ester (ThermoFisher, P36600) was reconstituted in dimethylsulfoxide
107 (DMSO; Sigma, D2650) to a final concentration of 10 mM/mL immediately before use. pHrodo
108 labeling dye was added to supernatant-free AB aggregates and mixed well. The reaction was
109 incubated in the dark at room temperature for 1 h. The reaction tube was centrifuged as described
110 and supernatant removed. To remove excess dye, 1 mL of cold methanol was added to the
111 aggregates and vortexed on high for 10 s. The reaction tube was centrifuged again, and the
112 supernatant removed. Aggregates were washed with 1 mL of Hank's Balanced Salt Solution (HBSS;

113 ThermoFisher, 14175095), vortexed on high for 10 seconds, and centrifuged before removing the
114 supernatant. The aggregates were washed an additional 3 times with HBSS as described. Finally, the
115 aggregates were resuspended in 200 uL HBSS, sonicated for 10 minutes, and stored at -20 C in
116 individual aliquots.

117 **Aβ phagocytosis assay**

118 iMGLs were collected between d40 – d42 of the differentiation and counted. iMGLs were then re-
119 plated in a minimum of 2 mL of conditioned maturation media on Matrigel hESC-qualified coated 6-
120 well plates and allowed to incubate overnight. pHrodo-labelled Aβ was thawed to room temperature
121 and resuspended by vortexing. Aβ was added at a dilution of 1:200 and incubated for 2 h. Plates
122 were then incubated on ice for 5 – 10 min to promote cell detachment of adherent cells. Cells were
123 collected and used for downstream applications.

124 **LPS stimulation**

125 iMGLs were collected between d38 – d39 of the differentiation and counted. iMGLs were then re-
126 plated in a minimum of 2 mL of conditioned maturation media on hESC-qualified Matrigel coated 6-
127 well plates and allowed to incubate overnight. iMGLs were treated with LPS (1 ug/mL; Thermo, 00-
128 4976-93) for 24 h. At the end of the 24 h incubation, plates were incubated on ice for 5 – 10 min to
129 promote cell detachment of adherent cells. iMGLs were collected and used for downstream
130 applications.

131 **Flow cytometry**

132 ***Extracellular protein staining***: After stimulation, iMGL were collected for extracellular flow cytometry
133 (FC) as described above. The buffer for fluorescence-activated cell sorting (FACS) was prepared by
134 diluting 30% BSA (Fisher Scientific, 50-203-6474) in DPBS to a final 2% solution. The buffer was
135 filtered through a 0.22 um filter system (Fisher, 09-761-107) and kept on ice. Cells were collected into

136 5 mL round-bottom tubes (Fisher, 14-959-1A) and the wells were washed once with DPBS and once
137 with 2% FACS buffer to collect any remaining cells. Cells were pelleted by centrifugation at 300 x g
138 for 5 min at 4 °C and supernatant was removed. Pelleted cells were washed twice with FACS buffer.
139 Supernatant was removed and the pelleted cells were resuspend in 100-200 uL FACS buffer. Cells
140 were then simultaneously treated with Human TruStain FcX according to the manufacturer's
141 instructions (Biologend; 422302) and stained with a live/dead dye (1:2500 in DPBS) on ice for 15 min.
142 Fluorophore-conjugated antibodies or their isotype controls were added to the cells and incubated in
143 the dark on ice for 30 min. Cells were washed twice with FACS buffer and centrifuged as described.
144 Stained cells were fixed with Fixation Buffer (Biolegend, 420801) according to the manufacturer's
145 instructions and washed twice with FACS buffer. Cells were either stained for intracellular (ICFC)
146 markers as described below or resuspended in 100-200 uL FACS buffer and immediately analyzed.
147 ***Intracellular protein staining***: If applicable, iMGLs were stained for intracellular flow cytometry
148 (ICFC) after FC staining. Fixed cells were washed twice with 5 mL FACS buffer followed by
149 permeabilization with Intracellular Staining Permeabilization Wash Buffer (Biolegend, 421002)
150 according to the manufacturer's instructions. Cells were stained with conjugated antibodies or their
151 isotype controls for 30 min in the dark at room temperature and washed twice with FACS buffer. Cells
152 were resuspended in the 100-200uL FACS buffer and immediately analyzed. All FC and ICFC data
153 were collected using the Sony SH800 Cell Sorter and flow cytometry data was analyzed using FlowJo
154 (v10). Compensation metrics were set using unstained and single-color compensation controls and
155 gating was determined using Fluorescence Minus One (FMOs) controls. All live/dead dyes,
156 conjugated antibodies, isotypes and their dilutions are listed in Table S1.

157 **Immunostaining**

158 iMGLs were collected between d40 – d42 of the differentiation and replated overnight on Matrigel-
159 coated Ibidi µ-Slide 8 Well ^{high} chamber slides (Ibidi, 80806) at a density of 50,000 – 75,000 iMGLs

160 per chamber. iMGLs were stimulated with LPS for 24 h or AB for 2 h and fixed with 4%
161 paraformaldehyde (PFA; Electron Microscopy Sciences, 15714-S) for 15 min at room temperature.
162 After washing three times with DPBS, iMGLs were permeabilized and blocked using 5% normal
163 donkey serum (Jackson Immuno Research, 017-000-121) with 0.02% Triton X-100 (Fisher,
164 BP151100) in PBS for 1 h at room temperature. iMGLs were then incubated with primary antibodies
165 diluted in blocking buffer at room temperature for 2 h. iMGLs were then washed three times with
166 DPBS and incubated with secondary antibodies diluted in a blocking buffer at room temperature for
167 45 min in the dark. If applicable, in staining panels containing two primary antibodies produced in
168 mouse or rabbit, the second primary antibody was conjugated to a 647 secondary using the Flexible
169 CoraLite Plus 647 Antibody Labeling Kit for Rabbit IgG (Proteintech, KFA003), Mouse IgG1
170 (Proteintech, KFA023), or Mouse IgG2a (Proteintech, KFA043) according to the manufacturer's
171 protocol. Following the last washing step after secondary incubation, iMGLs were stained with 674-
172 conjugated primaries for 2 h at room temperature in the dark. Cells were washed three times with
173 DPBS and then stained with Hoechst 33342 diluted 1:2000 in PBS before use (ThermoFisher; 62249)
174 for 3 min at room temperature in the dark. Cells were washed one final time and imaged using a
175 Nikon AX/AX R with NSPARC confocal microscope using Nikon NIS-Elements Imaging Software.
176 Primary antibodies used for immunofluorescence and dilutions are listed in Table S1. All secondary
177 antibodies were all used at a 1:1000 dilution in the blocking buffer and are listed in Table S1.

178 **Intracellular stress assays**

179 iMGLs were stimulated with LPS for 24 h or AB for 2 h using concentrations described above.
180 Staining for MitoSOX red (Thermo, M36008) and LipidTOX red (Thermo, H34476) was completed
181 according to the manufacturer's instructions. iMGLs were then fixed with 4% PFA for 15 min at room
182 temperature. iMGLs were washed three times with DPBS and then stained with Hoechst 33342
183 (ThermoFisher; 62249) diluted 1:2000 in PBS before use for 3 min at room temperature in the dark.

184 iMGLs were washed one final time and imaged using a Nikon AX/AX R with NSPARC confocal
185 microscope using Nikon NIS-Elements Imaging Software.

186 **Mesoscale multiplex biomarker assay**

187 iMGLs were replated in 2 mL of conditioned maturation media overnight prior to stimulation with LPS
188 for 24 h or Aβ for 2 h as described above. To assess multiple biomarkers, conditioned media from
189 each treatment condition was prepared and analyzed using the V-plex Human Biomarker 39-Plex Kit
190 (Mesoscale Discovery; K15209D-1) according to the manufacturer's protocol.

191 **Sample preparation, library construction, single-cell RNA sequencing, and data processing**

192 After stimulation with Aβ or LPS, single-cell suspensions were processed into sequencing-ready
193 libraries using the 10x Genomics Chromium Single Cell 3′ Platform. Libraries were sequenced on a
194 NovaSeq 6000 (Illumina) at a depth of 50k reads/cell. Following sequencing and FASTQ generation,
195 raw count matrices were produced using CellRanger v6.0.1. RNAs were mapped to the GRCh38
196 reference genome via STAR. Transcripts were assigned to individual cells and duplicate reads
197 removed. The resulting count matrices were processed using the Seurat (v5.3.0) package in R. We
198 applied quality controls metrics to the single-cell RNA sequencing results to remove cells with poor
199 transcriptomic quality (nCount_RNA >7500 & < 70,000; nFeatures_RNA >2500 & < 8,000; percent.mt
200 <10%; percent.rb to <30%). Seurat SCTransform function was used to normalize and scale the UMI
201 counts for each individual library based on regularized negative binomial regression. Principal
202 component analysis (PCA) was performed, followed by the FindNeighbors (dims = 1:10) and
203 FindClusters (res = 0.75) functions to identify clusters based on a shared nearest neighbor (SNN)
204 clustering algorithm. Finally, we performed UMAP dimension reduction (dims = 1:15). The data was
205 inspected for cell doublets using DoubletFinder (v2.0.4) and those containing mixed cluster

206 signatures were removed. Cell clusters were reprocessed using the functions described above prior
207 to in-depth analysis.

208 **Marker gene identification and cluster annotation**

209 We identified the top 200 differentially expressed genes (DEGs) for each of our 4 main clusters (padj
210 ≤ 0.05) using the FindAllMarkers function in Seurat (logfc.threshold = 1, min.cells.feature = 0.15, only
211 positive). We annotated each cluster based on the top 10 DEGs, sorted by descending order of log2
212 fold change. The Gene Ontology (GO) network for our 4 clusters was constructed using ClueGO
213 (v2.5.10) plugin in Cytoscape (v3.10.3). The analysis was performed using the
214 GO_BiologicalProcess-EBI-UniProt-GOA-ACAP-ARAP database (release 25.05.2022, 00:00). A two-
215 sided enrichment/depletion test was used to determine ontology enrichment with Bonferroni stepdown
216 correction (p ≤ 0.01) Parameters for network constructions were as follows: GO levels 3 – 8 with GO
217 term fusion to reduce redundant terms; Kappa score = 0.4; minimum genes included in term = 3;
218 minimum percentage of genes included in term = 4%. We also identified unique DEGs for our 13
219 subclsuters (padj ≤ 0.05) using the FindAllMarkers function in Seurat (logfc.threshold = 1,
220 min.cells.feature = 0.05).

221 **Gene ontology network analysis**

222 We compared Aβ and LPS-specific genes against the Unstimulated cluster using FindMarkers
223 (logfc.threshold = 0.1, min.cells.feature = 0.05) to identify treatment-specific DEGs. Genes with an
224 adjusted p value ≤ 0.05 were retained, and up- (avg_log2FC > 1) and down-regulated genes
225 (avg_log2FC < -1) were defined. ggplot2 was used to generate volcano plots. We identified enriched
226 GO networks (Biological Processes, Molecular Function, and Cellular Component using enrichGO
227 (v4.14.3) with the human reference annotation database (Org.Hs.eg.db).. Enrichment was performed

228 (maxGSSize = 500), and results were filtered for pathwayswith pval < 0.05. The top 20enriched and
229 underrepresented pathways were used to generate plots and scale set by Fold Enrichment.

230 **Prioritization of Alzheimer's Disease-associated genes expressed in microglia**

231 The prioritization of candidate genes was conducted using multiple criteria. These included the
232 selection of representative genes from each AD GWAS loci, as reported in the EADB GWAS, along
233 with genes with colocalization posterior probabilities (PP4) higher than 0.7, calculated using coloc,
234 against multiple eQTL/sQTL, including bulk RNA-seq across various brain tissues (MSBB, ROSMAP,
235 and Mayo Clinic), LCL RNA-seq, and sorted microglia RNA-seq(12,13). Genes reported in another
236 AD GWAS, with prioritization model probability higher than 0.5, and coloc results higher than 0.7
237 (across multiple eQTL datasets)(14). Genes identified in the colocalization results reported in the
238 MiGA study(15), which included four AD GWAS datasets(16–19) , along with transcriptome data
239 from in-vivo microglia eQTL(20) and ex-vivo microglia eQLT/sQTL from 4 brain regions (plus meta-
240 analysis). And finally, genes reported by the microglia-specific eQTL and caQTL study(21) that
241 applied multiple prioritization methods, including coloc, moloc(22), ABC model (23), and overlap with
242 microglia ATAC-seq peaks.

243 **Comparison to mouse and human microglia sets**

244 We applied SEURAT FindAllMarkers (logfc_threshold = -Inf, min.pct = 0.15) to contrast the
245 expression of cells in one iMGL subcluster vs. cells in remaining iMGL subclusters. This produced a
246 log2FC value and a p-value for each gene of MGLs. We then multiplied sign(log2FC) to -log10(p) for
247 each gene of each iMGL subcluster and applied GSEA with the 7 sets of rodent MG state markers
248 (2,24–30)and 12 sets of human MG state markers(31) as gene sets. Plotted is the sign (NES)*-
249 log10(p) from GSEA.

250 **Single-guide RNA (sgRNA) design, cloning and lentiviral library generation**

251 For each identified gene, three sgRNA targets were chosen between -50 and +300bp of the
252 transcriptional start site. Targets were chosen from top hits identified by CRISPick (Broad Institute)
253 and E-crisp (Boutros lab). In addition to 165 genes prioritized for analysis, sgRNAs targeting control
254 genes, CSF1R, CSF2RB, CDK8, and TGFBR2, previously identified as regulators of survival, as well
255 as non-targeting controls were included. The vector pCRISPRia-v2 was a gift from Jonathan
256 Weissman (Addgene 84832)(32). This was modified to express eGFP amplified from pXR001, a gift
257 from Patrick Hsu (Addgene 109049), in place of BFP by restriction digestion at the EcoRI and CsiI
258 sites and T4 ligation (NEB). Guide RNA sequences were appended with appropriate 5' and 3'
259 sequences, and a pool of oligonucleotides was synthesized (Twist Bioscience). The vector was
260 digested with BstXI and BlpI, and oligonucleotides were amplified by PCR and subsequently cloned
261 by Gibson assembly as previously described to generate an sgRNA library (33). Plasmids were
262 amplified and prepared by MaxiPrep for lentiviral generation as previously described(34). Lentivirus
263 was prepared by transfecting 293T cells in T75 flasks with the plasmid pool as well as psPAX2 and
264 pVSVg (Gifts from the Trono and Reya labs, Addgene 12260 and 14888, respectively) helper
265 plasmids using FuGene HD (Fisher, NC2132803).

266 **CRISPRi survival screen**

267 Human iPSCs constitutively expressing the CRISPRi construct dCas9-TagBFP-KRAB were
268 dissociated in Accutase and seeded into 6 well tissue culture-treated plates coated with Matrigel.
269 Cells were transduced with lentivirus at low MOI to generate cultures with 30% positive eGFP signal
270 and an average of at least 1000x sgRNA coverage. Cells were cultured overnight in the presence of
271 10μM Y-27632 and mTeSR Plus. Media was changed the following day. Cells were selected with
272 2μg/ml puromycin the next day for a duration of four days and allowed to recover without selection.
273 Cells were then seeded as small colonies in 15cm dishes for HPC differentiation and subsequent

274 iMGL differentiation as described above. Cells were collected and pelleted at days 0, 24, 36 and 45 of
275 differentiation. Pellets were subjected to gDNA extraction (Zymo).

276 **Sequencing and analysis of sgRNA distribution**

277 Genomic DNA was amplified with barcoded NGS primers as modified from (34) to include unique
278 indices on both forward and reverse primers as well as a 10nt variable region just upstream of the 5'
279 vector binding sequence. PCR reactions from each sample were pooled, and DNA was purified with
280 dual size selection with SPRI beads and analyzed on Fragment Analyzer. Sequencing libraries were
281 diluted and loaded onto Illumina iSeq 100. For CRISPR screening analysis, BCL files were converted
282 to FASTQ format. Raw reads were aligned to the reference with seqtk. Counts were then converted
283 to phenotype scores with MAGeCK-iNC pipeline modified so that two of the top three sgRNA
284 sequences per gene were analyzed(32). With this pipeline, comparisons between adjacent time
285 points day 12, day 24, day 36 and day 45 were made to assess the effect of gene knockdown at
286 different stages of iMGL differentiation and maturation. Heatmap displaying genes with significant
287 changes in abundance in at least one of these three intervals was made with ggplot2 in R. Epsilon
288 reflects abundance phenotype such that positive numbers reflect a reduction in corresponding gene-
289 targeting cell enrichment.

290 **Results**

291 **Benchmarking iMGL differentiation of dCas9-KRAB iPSC line against control ROSMAP iPSC**
292 **lines**

293 To ensure that the dCas9-KRAB iPSC line is suitable for downstream experiments, we first
294 benchmarked its microglial differentiation potential by comparing it to two in-house ROSMAP control
295 iPSC lines, BR09 and BR28 (8). All three iPSC lines were subjected to microglial differentiation using
296 published protocols (10,11), and quality control was performed at day 12 and day 40. Flow cytometry

297 analysis demonstrated comparable expression of CD43 and CD45 at both time points across all three
298 lines (sFig.1A), indicating similar differentiation trajectories.

299 We then further characterized the dCas9-KRAB line—the primary experimental line for this study—
300 using immunocytochemistry. The resulting iMGLs expressed key microglial markers, including PU.1,
301 IBA1, TREM2, P2RY2 and TREM119 (sFig.1B). qRT-PCR analysis validated the temporal expression
302 of microglia-relevant genes such as CD33, APOE, and TREM2 during differentiation (sFig.1C).
303 Functionally, these iMGLs exhibited Aβ phagocytosis upon exposure to pHrodo Red-labeled Aβ,
304 which was further enhanced upon LPS stimulation (sFig. 1D).

305 Together, these results demonstrate that the dCas9-KRAB iPSC line differentiates into functional
306 iMGLs with phenotypic and functional characteristics comparable to the control lines. This supports its
307 use for subsequent stimulation experiments, single-cell RNA sequencing, and the CRISPR-based
308 genetic screen.

309 **Aβ and LPS induce distinct morphological and marker expression changes in iMGLs**

310 To evaluate iMGL activation states in response to pathological stimuli, we treated cells with Aβ or LPS
311 and assessed morphological and marker expression changes using phase-contrast imaging and
312 immunostaining. Both Aβ and LPS treatments resulted in pronounced morphological changes
313 characterized by increased cellular processes and a transition to a multipolar morphology (Fig.1B).
314 These changes were particularly prominent under LPS treatment, which produced hypertrophic cells
315 with cytoplasmic granularity typical of classical microglial activation (Fig. 1B).

316 Immunostaining for IBA1 and CD45 confirmed activation-induced morphological changes. Notably, in
317 unstimulated iMGs, CD45 expression appeared localized to a small perinuclear cluster. Upon Aβ or
318 LPS stimulation, CD45 redistributed along the cell membrane, consistent with a shift in activation
319 status. We further quantified these morphological changes by measuring the proportion of cells

320 bearing processes longer than 3µm. Both Aβ- and LPS-treated conditions showed a significant
321 increase in the number of such cells compared to control, with the LPS condition exhibiting the
322 strongest effect (Fig. 1B).

323 **Single-cell RNA sequencing reveals stimulus-related iMGLs states**

324 To investigate how distinct stimuli shape the transcriptional landscape of human iMGLs, we
325 performed single-cell RNA sequencing (scRNA-seq) using the 10x Genomics Chromium platform on
326 control, Aβ-treated, and LPS-treated iMGLs. After quality control and filtering (sFig.2A), unsupervised
327 clustering revealed four major transcriptional clusters (Table S2), largely segregated by treatment
328 condition, yet all expressing core microglial identity genes such as *IRF1*, *PTPRC*, and *SPI1*,
329 confirming their microglial lineage (Fig. 1E, sFig2. B-C,).

330 Clusters 0 and 1 were predominantly composed of cells from the control and Aβ-treated conditions,
331 respectively. Cluster 0 expressed canonical microglial markers such as *P2RY12*, *FFAR4*, and
332 *CEBPA*, which are known markers of quiescent microglia and are typically downregulated under
333 neuroinflammatory stress. Cluster 1, which was enriched in Aβ-treated cells, showed elevated
334 expression of genes involved in lipid metabolism and tissue remodeling (*SCD4*, *CLDN1*, *PDGFB*), as
335 well as transcriptional regulators linked to immune adaptation and neuroinflammation, such as
336 *NR4A1*, *NR4A3*, and *IL23A (35–38)*. Cluster 2 was dominated by LPS-treated cells and characterized
337 by high expression of classical inflammatory and interferon-stimulated genes, including *CCL7*,
338 *MMP13*, and *MARCO*, suggesting a strong immune-activated state. Cluster 3 was composed of
339 proliferative iMGLs from both unstimulated and Aβconditions, marked by genes involved in cell cycle
340 and proliferation including *E2F8*, *TOP2A*, and *UBE2C*.

341 Gene Ontology (GO) enrichment analysis of the top 200 genes per cluster further supported the
342 functional divergence between clusters (Table S2). Cluster 1 (Aβ-enriched) showed enrichment for

343 pathways related to antigen processing, cell adhesion, and T-cell activation and differentiation.
344 Cluster 2 (LPS-enriched) was significantly enriched for immune response, chemotaxis, cytokine
345 production, and defense response pathways. Cluster 3 was strongly associated with cell cycle
346 transition and DNA repair processes. Although Cluster 0, which represents primarily unstimulated
347 iMGLs, does not dominate any single GO category, it nonetheless shows modest yet consistent
348 contributions across multiple biological processes, including defense response, cell proliferation, and
349 cellular activation. This pattern suggests that in the absence of external stimulation, iMGLs retain a
350 basal level of transcriptional activity related to homeostatic surveillance and immune readiness,
351 consistent with their physiological role as sentinels of the brain environment
352 These data demonstrate that Aβ and LPS elicit distinct transcriptional programs in iMGLs, with
353 partially overlapping yet stimulus-enriched activation states. This transcriptional diversity reflects the
354 capacity of iMGLs to mount tailored responses to different pathological cues and provides a
355 foundation for downstream integration with genetic perturbation data.

356 **Mapping iMGL states to mouse and human microglial states**

357 To contextualize our in vitro model with known in vivo iMGL diversity, we subclustered the four major
358 IMGL transcriptional clusters into 13 subclusters (Fig. 2A–B; Table S3) and systematically compared
359 them to reference microglial states from both mouse models (2,24–30). Among the reported mouse
360 microglia states, Aβ-associated subclusters were enriched for disease-associated microglia (DAM)
361 (10), neurodegeneration-associated microglia (MGnD) (30), and white matter-associated microglia
362 (WAM)(28). In contrast, LPS-associated subclusters showed strong alignment with interferon-
363 responsive microglia (RM) (25) and proliferative-region-associated microglia (PAM)(29), consistent
364 with pathways related to innate immune activation and cellular proliferation.

365 Mapping to published single-nucleus RNA-seq datasets from the human postmortem brain (31)
366 further supported stimulus-specific transcriptional signatures. Unstimulated clusters were primarily
367 aligned with ribosome biogenesis (MG3) and homeostatic microglia (MG0). Aβ-treated clusters
368 mapped to ribosome biogenesis (MG3), lipid processing (MG4), phagocytic (MG5), stress signature
369 (MG6), glycolytic (MG7), and inflammatory III (MG10) microglia. LPS clusters were mapped to
370 inflammatory I (MG2), glycolytic (MG7), inflammatory III (MG10), and cycling (MG12) microglia.
371 Clusters 12 and 13, which were derived from the major proliferative cluster (Cluster 3), also aligned
372 with cycling (MG12) microglia.

373 Together, these cross-species and cross-platform comparisons highlight that iMGLs are capable of
374 recapitulating disease-relevant microglial subtypes and preserving transcriptional heterogeneity in
375 response to distinct pathological stimuli.

376 To gain insight into the functional impact of Aβ and LPS exposure, we performed module score
377 analysis using curated gene sets from the Molecular Signatures Database (MSigDB)(39–42) related
378 to inflammation, stress response, and cell death (Table S3). Both Aβ and LPS increased cell death
379 (apoptosis, necroptosis, ferroptosis, pyroptosis), stress response (oxidative stress, integrated stress
380 response) and inflammatory phenotypes (IL6/IL10/IL27 signaling, INFɣ signaling and TGFβ signaling)
381 across multiple subclusters; however, the LPS condition showed a more pronounced increase in
382 those pathways. Interestingly, these cell stress, cell death and inflammatory pathways co-localized in
383 Aβ and LPS specific subclusters, suggesting a tightly coupled relationship between inflammatory
384 activation and cytotoxicity. The unstimulated and proliferative subclusters also demonstrated minimal
385 stress, inflammation, and cell death–related enrichment. These findings raise key mechanistic
386 questions about how microglia balance activation, stress adaptation, and survival in response to
387 pathologic insults such as Aβ and LPS.

388 **Differential gene expression analysis reveals shared and divergent molecular programs in Aβ-**
389 **and LPS-stimulated iMGLs**

390 To delineate the transcriptional responses of iMGLs to pathological stimuli, we performed differential
391 gene expression analysis comparing Aβ- and LPS-treated cells to unstimulated controls. Both
392 treatments induced substantial shifts in microglial identity, highlighted by the downregulation of key
393 homeostatic markers. Notably, *P2RY12* and *TREM2*, genes critical for maintaining homeostatic and
394 DAM-associated functions(43,44), were markedly suppressed in Aβ-treated cells and nearly
395 abolished under LPS stimulation (Fig. 3A). These findings indicate a profound reprogramming of
396 microglial state, with LPS eliciting a more extensive departure from the homeostatic transcriptome.

397 We next identified genes either commonly dysregulated across both stimuli or uniquely responsive to
398 Aβ or LPS (Fig. 3A; Table S4). GO term enrichment of shared upregulated genes revealed activation
399 of ferroptosis, lipid storage and transport, and inflammatory signaling pathways, including Toll-like
400 receptor (TLR) and NOD-like receptor (NLR) pathways—highlighting a convergent innate immune
401 and metabolic stress response. Conversely, shared downregulated genes were enriched for G-
402 protein-coupled receptor (GPCR) signaling, suggesting broad suppression of membrane signaling
403 and proteostasis (Fig. 3B; Table S4).

404 Aβ-specific transcriptional changes included upregulation of MAPK signaling, apoptotic processes,
405 interferon-γ and TNF response, cyclic AMP activity, and Golgi lumen acidification. These features
406 suggest a regulated stress response that may involve inflammatory signaling and enhanced
407 intracellular trafficking (Fig. 3C; Table S4). Interestingly, Aβ stimulation also led to upregulation of
408 pathways related to phagocytosis, suggesting engagement of clearance mechanisms potentially
409 relevant to Aβ processing (Fig. 3C; Table S4). By contrast, LPS-specific responses were
410 characterized by robust induction of cytokine signaling (e.g., IL-27, IL-15), detoxification, metal ion

411 sequestration, and apoptosis-related pathways (Fig. 3D, Table S4). Downregulated LPS-specific
412 pathways included MHC class II-mediated antigen presentation and T-cell activation (Fig. 3D, Table
413 S4), indicative of an innate-dominant inflammatory profile with suppressed adaptive immune features.

414 We further investigated the expression of key genes associated with distinct forms of programmed
415 cell death (PCD). Aβ or/and LPS stimulation induced upregulation of *CASP1, CASP4*, and *CASP5*,
416 consistent with activation of pyroptosis. However, the magnitude of upregulation varied:
417 *CASP5* showed minimal expression in unstimulated and Aβ-treated cells but was strongly induced in
418 the LPS condition. Similarly, *CASP1* and *CASP4* were modestly upregulated in Aβ-treated iMGLs and
419 more robustly elevated under LPS stimulation (Figure 3E). These caspases are central to
420 inflammasome activation and cytokine processing, a hallmark of pyroptotic cell death(45–49) . We
421 also observed differential activation of apoptotic pathways. *CASP3* was mildly upregulated in both Aβ-
422 and LPS-treated cells but *CASP7* exhibited a pronounced increase exclusively in LPS-treated cells.
423 These executioner caspases mediate downstream apoptotic processes including DNA fragmentation
424 and membrane blebbing (50,51). Regarding ferroptosis, we detected significant upregulation of
425 *ACSL4*, *TFRC*, *FTH1*, and *PTGS2* in both Aβ- and LPS-treated conditions, but again with stronger
426 induction under LPS stimulation. These genes are involved in lipid metabolism and iron homeostasis,
427 which sensitize cells to ferroptosis(52–55). *GPX4*, a central negative regulator of ferroptosis that
428 detoxifies lipid hydroperoxides(56,57), was downregulated under both conditions, but the suppression
429 was more modest in the Aβ-treated cells. This expression pattern supports activation of ferroptotic
430 stress, particularly in the LPS condition. In addition, we observed increased expression of *RIPK1* and
431 *MLKL*, key mediators of necroptosis(58,59), in LPS-treated cells, with a mild elevation of *RIPK1* also
432 noted in Aβ-treated cells. Altogether, these findings suggest coordinated activation of multiple PCD
433 mechanisms, with LPS inducing a more potent and multifaceted response than Aβ.

434 Together, these findings demonstrate that Aβ and LPS induce overlapping but distinct molecular
435 programs in iMGLs. While both stimuli activate inflammatory and PCD pathways, Aβ elicits a more
436 controlled response involving MAPK signaling, vesicular trafficking, and phagocytosis, whereas LPS
437 drives widespread innate immune activation with suppression of adaptive immune signaling. This
438 divergence highlights the context-specific nature of microglial responses to different pathological
439 insults.

440 **Cellular assays confirmed Aβ- and LPS-induced cellular stress and inflammatory responses**

441 To validate the transcriptional phenotypes identified in our single-cell analysis, we performed a series
442 of cellular and molecular assays in iMGLs under unstimulated, Aβ-, and LPS-treated conditions.
443 Immunofluorescence staining for cleaved caspase-3, a marker of apoptosis, revealed increased
444 staining in both Aβ- and LPS-treated cells compared to controls, aligning with the upregulation of
445 apoptotic genes and gene modules. LPS treatment induced a more robust apoptotic response than
446 Aβ, which showed a modest, non-significant increase (Fig. 4A).

447 To assess oxidative stress, we used MitoSOX staining to detect mitochondrial superoxide production.
448 MitoSOX is a mitochondrial-targeted fluorogenic dye that selectively reacts with superoxide,
449 generating red fluorescence that serves as a readout of mitochondrial oxidative stress. While
450 unstimulated cells showed minimal signal, Aβ-treated cells exhibited diffuse cytoplasmic staining with
451 some perinuclear accumulation (Fig. 4A). By contrast, LPS-treated cells showed punctate signals
452 concentrated in the soma and processes (Fig. 4A). Both treatments led to an increased proportion of
453 MitoSOX^{+} cells, which was more pronounced with LPS (Fig. 4A), indicating elevated mitochondrial
454 ROS production.

455 Similarly, we applied LipidTOX staining to assess lipid peroxidation. LipidTOX dyes detect neutral
456 lipids and are commonly used to monitor lipid droplet accumulation and oxidative lipid damage.

457 Elevated LipidTOX signal reflects increased lipid peroxidation, a hallmark of ferroptosis(60). Indeed,
458 LipidTOX staining revealed enhanced lipid peroxidation in both Aβ- and LPS-treated iMGLs (Fig. 4A),
459 consistent with transcriptional signatures indicative of ferroptosis activation.

460 We next examined lysosomal activation using CD68 immunostaining and flow cytometry. Both
461 treatments increased CD68 expression relative to controls, suggesting enhanced lysosomal stress.
462 Flow cytometry further confirmed this elevation and revealed differential expression patterns of
463 activation markers (Fig. 4A, 4B). Aβ-treated microglia upregulated TREM2, while LPS treatment
464 reduced its expression (Fig. 4B). CD38, in contrast, was specifically upregulated by LPS, with no
465 notable change in Aβ-treated cells (Fig. 4B), indicating stimulus-specific immune activation states.

466 Finally, multiplex cytokine profiling confirmed the distinct inflammatory responses triggered by each
467 condition. Aβ stimulation led to the selective secretion of chemokines such as CCL3 and CCL4, while
468 LPS induced a broader pro-inflammatory signature, including elevated levels of multiple cytokines
469 and chemokines (Fig. 4C; Table S5).

470 Together, these findings confirm that Aβ and LPS induce overlapping yet distinct stress and
471 inflammatory responses in iMGLs. Both stimuli activate oxidative, lysosomal, and immune pathways,
472 with LPS driving a more extensive cytotoxic and inflammatory program.

473 **CRISPRi functional screening reveals partial overlap between AD-risk genes and microglial**
474 **stress response genes**

475 To build on our finding that Aβ and LPS induce microglial PCD through multiple stress programs—
476 including apoptosis, pyroptosis, ferroptosis, and necroptosis —we sought to identify genetic
477 regulators of microglial survival under baseline differentiation conditions. We focused on 168
478 microglial genes implicated in Alzheimer's disease risk by GWAS and fine-mapping studies (16–19).

479 We first examined their expression across unstimulated, Aβ-, and LPS-treated iMGLs in our single-
480 cell dataset. A distinct pattern of transcriptional responses emerged, with 127 AD-associated genes
481 differentially expressed in a condition-specific manner (Fig. 5B). This suggested that a subset of
482 these genes might contribute to the microglial stress response and cell viability.

483 To functionally assess knockdown impact, we first targeted the AD risk gene CD33 using individual
484 lentiviral constructs. CD33 expression was significantly reduced at both the transcript and protein
485 levels, confirming effective targeting by two independent sgRNAs (Fig. 5C–E). We then proceeded to
486 clone all sgRNAs targeting the 168 genes into pooled lentiviral vectors (Table S6). These pooled
487 libraries were transduced into iPSCs prior to iMGLs differentiation, and sgRNA representation was
488 quantified at four key timepoints (D0, D12, D24, D36, and D45) via PCR amplification and next-
489 generation sequencing (Fig. 5A). Initial distribution analysis confirmed an appropriate sgRNA
490 distribution at the iPSC stage as described [32] (Fig. 5G). To reduce the confounding effects of
491 differentiation-associated gene expression changes, we compared sgRNA abundance between two
492 consecutive timepoints (D24 vs D12, d36 vs d24, and D45 vs d36). This strategy minimizes temporal
493 bias and enables more accurate identification of genes involved in iMGL survival. We identified 38
494 genes regulating iMGL survival (Fig. 5G; Table S6), 31 of which were also expressed in the scRNA-
495 seq dataset. These genes were classified into pro-survival, anti-survival, and dynamic
496 regulators based on temporal and directional effects (Fig. 5I-J).

497 To explore the relationship between transcriptional stress responses and survival, we compared
498 differentially expressed genes in Aβ- and LPS-treated iMGLs with the 31 candidate survival regulators
499 identified from our genetic screen. Among 127 genes differentially expressed under either treatment,
500 27 overlapped with survival-related genes, and 17 were shared across Aβ-responsive, LPS-
501 responsive, and survival-linked categories. (Fig. 5H, Table S6). Interestingly, LPS treatment led to a
502 general downregulation of both pro-survival and anti-survival genes, except for *TREM1*, which was

503 strongly upregulated and classified as anti-survival. By contrast, Aβ treatment induced moderate
504 upregulation of several pro-survival (*COX7C*, *CSF2RB*, *PLEKHA1*), anti-survival (*PHB, PICALM*) and
505 dynamic-expression (*FIBP, SPI1*) genes (Fig. 5I–J). These patterns align with the more pronounced
506 cytotoxicity seen in LPS-treated cells and suggest that Aβ may activate compensatory survival
507 programs.

508 his intersection supports the idea that a fraction of AD-associated microglial genes influence stress
509 response and survival, highlighting key candidates for future mechanistic studies aiming to connect
510 AD genetics to microglial viability under disease-relevant conditions.

511 **Discussion**

512 Our study reveals that human iPSC-derived microglia like cells (iMGLs) exhibit distinct and
513 overlapping transcriptional and functional responses to two key stressors—Aβ and LPS—which
514 represent Alzheimer's disease-associated and classical inflammatory insults, respectively. Both
515 treatments induce pronounced cellular stress, immune activation, and features of programmed cell
516 death (PCD), including apoptosis, pyroptosis, and ferroptosis. However, LPS treatment elicits a
517 broader pro-inflammatory and cytotoxic response, whereas Aβ triggers a more specific set of gene
518 programs. This distinction is supported by module score analysis using curated gene sets (Fig.s 2E),
519 differential gene expression and pathway analysis (Fig. 3) and cellular assays (Fig. 4).

520 Through a pooled CRISPRi screen targeting 168 AD-associated microglial genes, we identified 31
521 genes that regulate iMGL survival during differentiation. Notably, 27 of these 31 genes were also
522 differentially expressed in response to Aβ or LPS treatment, revealing a partial overlap between
523 stress-induced transcriptional changes and intrinsic pro-survival and anti-survival programs (Fig. 5).
524 These findings suggest that the transcriptional stress response may either promote adaptive survival
525 or drive degeneration depending on the context and specific genes engaged.

526 The overlap between stress-responsive and survival-regulating genes also aligns with the emerging
527 literature on microglial PCD as a critical regulatory mechanism in the CNS. Apoptosis, pyroptosis,
528 necroptosis and ferroptosis have all been observed in microglia under various pathological conditions,
529 including neurodegeneration and CNS injury (61,62) . Dysregulation of these pathways can result in
530 excessive inflammation and tissue damage, contributing to disease progression in a feedforward
531 manner (62–64). Our data reinforce this concept by demonstrating that microglial stress responses,
532 when unresolved, may trigger programmed cell death pathways that could exacerbate
533 neurodegeneration.

534 Importantly, our results build on prior studies using iMGLs as models of human disease. Notably,
535 Dolan et al. demonstrated that iMGLs recapitulate key transcriptional states of disease-associated
536 microglia (DAM) under stress conditions, including Aβ exposure (65). Our findings are consistent with
537 and extend this work by adding functional dimensions—specifically cell survival regulation—and
538 highlighting the utility of iMGLs for genetic perturbation studies. Compared to previous CRISPR
539 screens(32) that focused on druggable genes, our approach integrates disease-relevant gene
540 selection with developmental timing, offering new insights into microglial vulnerabilities and resilience
541 mechanisms.

542 Collectively, these data position iPSC-derived iMGLs as a powerful and tractable model to interrogate
543 human microglial states under disease-relevant stressors. They also point to new directions for
544 therapeutic discovery, particularly targeting stress-modulated survival pathways to enhance microglial
545 fitness and slow neurodegenerative progression.

546 **Conclusion**

547 This study provides a multifaceted view of how iMGLs respond to stressors relevant to AD and
548 inflammation. By integrating single-cell transcriptomics, cellular assays, and a pooled CRISPRi

549 survival screen, we show that Aβ and LPS induce both shared and distinct molecular responses,
550 including stress, immune and PCD pathways. These responses are functionally linked to a subset of
551 AD-associated microglial genes, some of which regulate microglial viability. Our findings underscore
552 the dual role of microglia as stress sensors and effectors of cell fate and demonstrate that adaptive
553 versus degenerative responses are driven by distinct transcriptional programs. This work not only
554 advances our understanding of microglial biology in neurodegeneration but also lays a foundation for
555 identifying and modulating gene pathways that promote microglial resilience. Future efforts should
556 aim to mechanistically dissect pro-survival versus pro-death modules and explore therapeutic
557 strategies that fine-tune microglial adaptation under stress.

558 **Limitations**

559 While our findings provide valuable insights into microglial stress responses and survival programs,
560 several limitations should be noted. First, the CRISPRi screen was performed under baseline
561 differentiation conditions without exposure to Aβ or LPS, limiting our ability to identify condition-
562 specific survival regulators. Future context-dependent screens could more precisely map genes
563 involved in stress-specific adaptation. Second, although iPSC-derived iMGLs recapitulate many
564 transcriptional and functional aspects of primary human microglia—including disease-associated
565 states—they do not fully mimic the CNS environment, lacking interactions with neurons, astrocytes,
566 and vasculature. This may impact the generalizability of observed responses. Third, the gene set
567 used in the screen was focused on AD-associated genes and may not capture broader regulators of
568 microglial homeostasis or stress resilience. Finally, while gene expression and functional overlap
569 suggest possible regulatory roles, transcriptional induction does not confirm causality. Future
570 mechanistic studies will be necessary to validate the direct contribution of candidate genes to
571 microglial stress handling and survival.

572 **List of abbreviations**

573 **Aβ**: amyloid beta

574 **LPS**: lipopolysaccharide

575 **AD**: Alzheimer's Disease

576 **iMGLs**: human induced pluripotent stem cell-derived microglia-like cells

577 **MAP**: Rush Memory and Aging Project

578 **sgRNAs:** singe-guide RNAs

579 **CRISPRi**: CRISPR interference

580 **scRNA-seq**: single-cell RNA sequencing

581 **GO**: Gene Ontology

582 **DAM**: disease-associated microglia

583 **MGnD**: neurodegeneration-associated microglia

584 **WAM**: white matter-associated microglia

585 **IRM**: interferon-responsive microglia

586 **PAM**: proliferative-region-associated microglia

587 **MSigDB**: Molecular Signatures Database

588 **TLR**: Toll-like receptor

589 **NLR**: NOD-like receptor

590 **GPCR**: G-protein-coupled receptor

591 **PCD**: programmed cell death

592 **FC**: flow cytometry

593 **FACS**: fluorescence-activated cell sorting

594

595

596

597 **Declarations**

598 **Ethics approval and consent to participate**

599 Two iPSC lines (BR09 and BR28) were obtained through the Rush Memory and Aging Project (MAP)
600 cohort study at the Rush Alzheimer's Disease Center, Rush University Medical Center (RUMC),
601 Chicago, IL., in compliance with national ethical guidelines. All MAP participants agreed to annual
602 clinical evaluation, blood draw, and brain donation. MAP was approved by the Institutional Review
603 Board of RUMC. All participants signed an informed and repository consent and an Anatomic Gift Act
604 for brain donation.

605 **Availability of data and materials**

606 We generated raw and normalized count matrices of the single-cell RNA sequencing and CRISPR
607 interference screen datasets from the dCas9-KRAB line. These data are available at GEO under
608 accession code GSE306200 & GSE306202.

609 **Competing interest**

610 The authors declare that they have no competing interests

611 **Funding**

612 This study was supported by NIA grants R01AG074082 and R01AG079223 (to Y.W.), P30AG10161,
613 P30AG72975, R01AG015819, R01AG017917, U01AG61356 and the Paul M Angell Family
614 Foundation (to D. A. B.).

615 **Author contributions**

616 E.M.C established the iMGL differentiation protocol in-house based on published methods. D.S.
617 performed cellular assay validation experiments and conducted single-cell RNA sequencing data

618 analysis. F.S. carried out the CRISPR interference screen and performed subsequent data analysis.
619 R.A.V. selected AD-associated microglial genes for CRISPR screening. B.N. contributed to microglial
620 state mapping analysis. N.A.K. and H.V. assisted with assay development. D.S., N.A.K. and S.D.T.
621 conducted single-cell RNA sequencing experiments, and J.X. performed data processing. D.S.
622 drafted the initial version of the manuscript and Y.W. substantially revised and finalized the
623 manuscript. D.A.B. provided insightful and critical feedback and input. Y.W. conceived and directed
624 the study, led the research activities, and supervised manuscript preparation. All authors reviewed
625 and approved the final manuscript.

626 **Acknowledgments**

627 We thank the thesis committee of Dr. Devin Saunders, including Dr. Jeffrey H. Kordower, Dr.
628 Jennillee Wallace, Dr. Xiu-Ti Hu, and Dr. David Bennett, for their insightful feedback and input. We
629 also acknowledge the support of all RADC staff for their assistance throughout this project. This
630 research was made possible through the Allen Cell Collection, available from the Coriell Institute for
631 Medical Research.

632 **Authors' Information**

633 Further information and requests may be directed to the corresponding author Dr. Yanling Wang
634 (Yanling_Wang@rush.edu)

635 **Materials Availability**

636 This study did not generate new unique reagents.

637

638

639 **References**

640 1. Frank MG, Fonken LK, Watkins LR, Maier SF. Microglia: Neuroimmune-sensors of stress. Semin
641 Cell Dev Biol. 2019 Oct;94:176–85.

642 2. Deczkowska A, Keren-Shaul H, Weiner A, Colonna M, Schwartz M, Amit I. Disease-associated
643 microglia: A universal immune sensor of neurodegeneration. Cell. 2018 May 17;173(5):1073–81.

644 3. Colonna M, Butovsky O. Microglia function in the central nervous system during health and
645 neurodegeneration. Annu Rev Immunol. 2017 Apr 26;35:441–68.

646 4. Gao C, Jiang J, Tan Y, Chen S. Microglia in neurodegenerative diseases: mechanism and
647 potential therapeutic targets. Signal Transduct Target Ther. 2023 Sep 22;8(1):359.

648 5. Zhang W, Xiao D, Mao Q, Xia H. Role of neuroinflammation in neurodegeneration development.
649 Signal Transduct Target Ther. 2023 Jul 12;8(1):267.

650 6. Hickman S, Izzy S, Sen P, Morsett L, El Khoury J. Microglia in neurodegeneration. Nat Neurosci.
651 2018 Oct;21(10):1359–69.

652 7. Hansen DV, Hanson JE, Sheng M. Microglia in Alzheimer's disease. J Cell Biol. 2018 Feb
653 5;217(2):459–72.

654 8. Lagomarsino VN, Pearse RV 2nd, Liu L, Hsieh YC, Fernandez MA, Vinton EA, et al. Stem cell-
655 derived neurons reflect features of protein networks, neuropathology, and cognitive outcome of
656 their aged human donors. Neuron. 2021 Nov 3;109(21):3402–20.e9.

657 9. Bennett DA, Buchman AS, Boyle PA, Barnes LL, Wilson RS, Schneider JA. Religious Orders
658 Study and Rush Memory and Aging Project. J Alzheimers Dis. 2018;64(s1):S161–89.

659 10. Abud EM, Ramirez RN, Martinez ES, Healy LM, Nguyen CHH, Newman SA, et al. iPSC-Derived
660 Human Microglia-like Cells to Study Neurological Diseases. Neuron. 2017 Apr 19;94(2):278–
661 93.e9.

662 11. McQuade A, Coburn M, Tu CH, Hasselmann J, Davtyan H, Blurton-Jones M. Development and
663 validation of a simplified method to generate human microglia from pluripotent stem cells. Mol
664 Neurodegener. 2018 Dec 22;13(1):67.

665 12. Bellenguez C, EADB. TopMed-imputed genome-wide association study of Alzheimer's disease in
666 more than 100,000 European samples from the EADB project. Alzheimers Dement [Internet].
667 2020 Dec;16(S3). Available from: http://dx.doi.org/10.1002/alz.037971

668 13. Giambartolomei C, Vukcevic D, Schadt EE, Franke L, Hingorani AD, Wallace C, et al. Bayesian
669 test for colocalisation between pairs of genetic association studies using summary statistics.
670 PLoS Genet. 2014 May;10(5):e1004383.

671 14. Schwartzentruber J, Cooper S, Liu JZ, Barrio-Hernandez I, Bello E, Kumasaka N, et al. Genome-
672 wide meta-analysis, fine-mapping and integrative prioritization implicate new Alzheimer's disease
673 risk genes. Nat Genet. 2021 Mar;53(3):392–402.

674 15. Lopes K de P, Snijders GJL, Humphrey J, Allan A, Sneeboer MAM, Navarro E, et al. Genetic
675 analysis of the human microglial transcriptome across brain regions, aging and disease
676 pathologies. Nat Genet. 2022 Jan;54(1):4–17.

677 16. Kunkle BW, Grenier-Boley B, Sims R, Bis JC, Damotte V, Naj AC, et al. Genetic meta-analysis of
678 diagnosed Alzheimer's disease identifies new risk loci and implicates Aβ, tau, immunity and lipid
679 processing. Nat Genet. 2019 Mar;51(3):414–30.

680 17. Marioni RE, Harris SE, Zhang Q, McRae AF, Hagenaars SP, Hill WD, et al. GWAS on family
681 history of Alzheimer's disease. Transl Psychiatry. 2018 May 18;8(1):99.

682 18. Lambert JC, Ibrahim-Verbaas CA, Harold D, Naj AC, Sims R, Bellenguez C, et al. Meta-analysis
683 of 74,046 individuals identifies 11 new susceptibility loci for Alzheimer's disease. Nat Genet. 2013
684 Dec;45(12):1452–8.

685 19. Jansen IE, Savage JE, Watanabe K, Bryois J, Williams DM, Steinberg S, et al. Genome-wide
686 meta-analysis identifies new loci and functional pathways influencing Alzheimer's disease risk.
687 Nat Genet. 2019 Jan 7;51(3):404–13.

688 20. Young AMH, Kumasaka N, Calvert F, Hammond TR, Knights A, Panousis N, et al. A map of
689 transcriptional heterogeneity and regulatory variation in human microglia. Nat Genet. 2021
690 Jun;53(6):861–8.

691 21. Kosoy R, Fullard JF, Zeng B, Bendl J, Dong P, Rahman S, et al. Genetics of the human microglia
692 regulome refines Alzheimer's disease risk loci. Nat Genet. 2022 Aug;54(8):1145–54.

693 22. Giambartolomei C, Zhenli Liu J, Zhang W, Hauberg M, Shi H, Boocock J, et al. A Bayesian
694 framework for multiple trait colocalization from summary association statistics. Bioinformatics.
695 2018 Aug 1;34(15):2538–45.

696 23. Fulco CP, Nasser J, Jones TR, Munson G, Bergman DT, Subramanian V, et al. Activity-by-
697 contact model of enhancer-promoter regulation from thousands of CRISPR perturbations. Nat
698 Genet. 2019 Dec;51(12):1664–9.

699 24. Keren-Shaul H, Spinrad A, Weiner A, Matcovitch-Natan O, Dvir-Szternfeld R, Ulland TK, et al. A
700 unique microglia type associated with restricting development of Alzheimer's disease. Cell. 2017
701 Jun;169(7):1276–90.e17.

702 25. Roy ER, Chiu G, Li S, Propson NE, Kanchi R, Wang B, et al. Concerted type I interferon signaling
703 in microglia and neural cells promotes memory impairment associated with amyloid β plaques.
704 Immunity. 2022 May 10;55(5):879–94.e6.

705 26. Marschallinger J, Iram T, Zardeneta M, Lee SE, Lehallier B, Haney MS, et al. Lipid-droplet-
706 accumulating microglia represent a dysfunctional and proinflammatory state in the aging brain.
707 Nat Neurosci. 2020 Feb;23(2):194–208.

708 27. Clayton K, Delpech JC, Herron S, Iwahara N, Ericsson M, Saito T, et al. Plaque associated
709 microglia hyper-secrete extracellular vesicles and accelerate tau propagation in a humanized
710 APP mouse model. Mol Neurodegener. 2021 Mar 22;16(1):18.

711 28. Safaiyan S, Besson-Girard S, Kaya T, Cantuti-Castelvetri L, Liu L, Ji H, et al. White matter aging
712 drives microglial diversity. Neuron. 2021 Apr 7;109(7):1100–17.e10.

713 29. Li Q, Cheng Z, Zhou L, Darmanis S, Neff NF, Okamoto J, et al. Developmental heterogeneity of
714 microglia and brain myeloid cells revealed by deep single-cell RNA sequencing. Neuron. 2019
715 Jan 16;101(2):207–23.e10.

716 30. Krasemann S, Madore C, Cialic R, Baufeld C, Calcagno N, El Fatimy R, et al. The TREM2-APOE
717 pathway drives the transcriptional phenotype of dysfunctional microglia in neurodegenerative
718 diseases. Immunity. 2017 Sep 19;47(3):566–81.e9.

719 31. Sun N, Victor MB, Park YP, Xiong X, Scannail AN, Leary N, et al. Human microglial state
720 dynamics in Alzheimer's disease progression. Cell. 2023 Sep 28;186(20):4386–403.e29.

721 32. Dräger NM, Sattler SM, Huang CTL, Teter OM, Leng K, Hashemi SH, et al. A CRISPRi/a platform
722 in human iPSC-derived microglia uncovers regulators of disease states. Nat Neurosci. 2022
723 Sep;25(9):1149–62.

724 33. Horlbeck MA, Gilbert LA, Villalta JE, Adamson B, Pak RA, Chen Y, et al. Compact and highly
725 active next-generation libraries for CRISPR-mediated gene repression and activation. Elife
726 [Internet]. 2016 Sep 23;5. Available from: http://dx.doi.org/10.7554/eLife.19760

727 34. Joung J, Konermann S, Gootenberg JS, Abudayyeh OO, Platt RJ, Brigham MD, et al. Genome-
728 scale CRISPR-Cas9 knockout and transcriptional activation screening. Nat Protoc. 2017 Mar
729 23;12(4):828–63.

730 35. Phelan DE, Shigemura M, Aldhafiri S, Mota C, Hall TJ, Sznajder JI, et al. Transcriptional profiling
731 of monocytes deficient in nuclear orphan receptors NR4A2 and NR4A3 reveals distinct signalling
732 roles related to antigen presentation and viral response. Front Immunol. 2021 Jun 25;12:676644.

733 36. Rothe T, Ipseiz N, Faas M, Lang S, Perez-Branguli F, Metzger D, et al. The nuclear receptor
734 Nr4a1 acts as a microglia rheostat and serves as a therapeutic target in autoimmune-driven
735 central nervous system inflammation. J Immunol. 2017 May 15;198(10):3878–85.

736 37. Zhao Y, Bruemmer D. NR4A orphan nuclear receptors: transcriptional regulators of gene
737 expression in metabolism and vascular biology. Arterioscler Thromb Vasc Biol. 2010
738 Aug;30(8):1535–41.

739 38. García-Domínguez M. The role of IL-23 in the development of inflammatory diseases. Biology
740 (Basel). 2025 Mar 27;14(4):347.

741 39. Subramanian A, Tamayo P, Mootha VK, Mukherjee S, Ebert BL, Gillette MA, et al. Gene set
742 enrichment analysis: a knowledge-based approach for interpreting genome-wide expression
743 profiles. Proc Natl Acad Sci U S A. 2005 Oct 25;102(43):15545–50.

744 40. Castanza AS, Recla JM, Eby D, Thorvaldsdóttir H, Bult CJ, Mesirov JP. Extending support for
745 mouse data in the Molecular Signatures Database (MSigDB). Nat Methods. 2023
746 Nov;20(11):1619–20.

747 41. Liberzon A, Subramanian A, Pinchback R, Thorvaldsdóttir H, Tamayo P, Mesirov JP. Molecular

748 signatures database (MSigDB) 3.0. Bioinformatics. 2011 Jun 15;27(12):1739–40.

749 42. Liberzon A, Birger C, Thorvaldsdóttir H, Ghandi M, Mesirov JP, Tamayo P. The Molecular
750 Signatures Database (MSigDB) hallmark gene set collection. Cell Syst. 2015 Dec 23;1(6):417–
751 25.

752 43. Li Y, Xu H, Wang H, Yang K, Luan J, Wang S. TREM2: Potential therapeutic targeting of
753 microglia for Alzheimer's disease. Biomed Pharmacother. 2023 Sep;165(115218):115218.

754 44. Lin SS, Tang Y, Illes P, Verkhratsky A. The safeguarding microglia: Central role for P2Y12
755 receptors. Front Pharmacol. 2020;11:627760.

756 45. Man SM, Karki R, Kanneganti TD. Molecular mechanisms and functions of pyroptosis,
757 inflammatory caspases and inflammasomes in infectious diseases. Immunol Rev. 2017
758 May;277(1):61–75.

759 46. Liu B, He R, Zhang L, Hao B, Jiang W, Wang W, et al. Inflammatory caspases drive pyroptosis in
760 acute lung injury. Front Pharmacol. 2021 Feb 5;12:631256.

761 47. Liang Y, Song P, Chen W, Xie X, Luo R, Su J, et al. Inhibition of caspase-1 ameliorates ischemia-
762 associated blood-brain barrier dysfunction and integrity by suppressing pyroptosis activation.
763 Front Cell Neurosci. 2020;14:540669.

764 48. Wu X, Wan T, Gao X, Fu M, Duan Y, Shen X, et al. Microglia pyroptosis: A candidate target for
765 neurological diseases treatment. Front Neurosci. 2022 Jul 22;16:922331.

766 49. Al Mamun A, Geng P, Wang S, Shao C. Role of pyroptosis in endometrial cancer and its
767 therapeutic regulation. J Inflamm Res. 2024 Oct 3;17:7037–56.

768 50. Hartmann A, Hunot S, Michel PP, Muriel MP, Vyas S, Faucheux BA, et al. Caspase-3: A
769 vulnerability factor and final effector in apoptotic death of dopaminergic neurons in Parkinson's
770 disease. Proc Natl Acad Sci U S A. 2000 Mar 14;97(6):2875–80.

771 51. Walsh JG, Cullen SP, Sheridan C, Lüthi AU, Gerner C, Martin SJ. Executioner caspase-3 and
772 caspase-7 are functionally distinct proteases. Proc Natl Acad Sci U S A. 2008 Sep
773 2;105(35):12815–9.

774 52. Jiang X, Stockwell BR, Conrad M. Ferroptosis: mechanisms, biology and role in disease. Nat Rev
775 Mol Cell Biol. 2021 Apr;22(4):266–82.

776 53. Tian R, Abarientos A, Hong J, Hashemi SH, Yan R, Dräger N, et al. Genome-wide CRISPRi/a
777 screens in human neurons link lysosomal failure to ferroptosis. Nat Neurosci. 2021 May 24;1–15.

778 54. Xie LH, Fefelova N, Pamarthi SH, Gwathmey JK. Molecular mechanisms of ferroptosis and
779 relevance to cardiovascular disease. Cells. 2022 Sep 1;11(17):2726.

780 55. Liu S, Gao X, Zhou S. New target for prevention and treatment of neuroinflammation: Microglia
781 iron accumulation and ferroptosis. ASN Neuro. 2022 Jan;14:17590914221133236.

782 56. Li Y, Xiao D, Wang X. The emerging roles of ferroptosis in cells of the central nervous system.
783 Front Neurosci. 2022 Dec 14;16:1032140.

784 57. Ma T, Du J, Zhang Y, Wang Y, Wang B, Zhang T. GPX4-independent ferroptosis-a new strategy
785 in disease's therapy. Cell Death Discov. 2022 Oct 30;8(1):434.

786 58. Chai Z, Ma T, Li Y, Chen Q, Kang Y, Sun J, et al. Inhibition of inflammatory factor TNF-α by
787 ferrostatin-1 in microglia regulates necroptosis of oligodendrocyte precursor cells. Neuroreport.
788 2023 Aug 24;34(11):583–91.

789 59. Li L, Tong A, Zhang Q, Wei Y, Wei X. The molecular mechanisms of MLKL-dependent and
790 MLKL-independent necrosis. J Mol Cell Biol. 2021 Apr 10;13(1):3–14.

791 60. Do Q, Xu L. How do different lipid peroxidation mechanisms contribute to ferroptosis? Cell Rep
792 Phys Sci. 2023 Dec 20;4(12):101683.

793 61. Cai L, Fan Q, Pang R, Chen C, Zhang Y, Xie H, et al. Microglia programmed cell death in
794 neurodegenerative diseases and CNS injury. Apoptosis. 2025 Feb;30(1-2):446–65.

795 62. Qiu Z, Zhang H, Xia M, Gu J, Guo K, Wang H, et al. Programmed death of microglia in
796 Alzheimer's disease: Autophagy, ferroptosis, and pyroptosis. J Prev Alzheimers Dis.
797 2023;10(1):95–103.

798 63. Thadathil N, Nicklas EH, Mohammed S, Lewis TL Jr, Richardson A, Deepa SS. Necroptosis
799 increases with age in the brain and contributes to age-related neuroinflammation [Internet].
800 bioRxiv. bioRxiv; 2021. Available from: http://dx.doi.org/10.1101/2021.07.23.453580

801 64. Moujalled D, Strasser A, Liddell JR. Molecular mechanisms of cell death in neurological diseases.
802 Cell Death Differ. 2021 Jul;28(7):2029–44.

803 65. Dolan MJ, Therrien M, Jereb S, Kamath T, Gazestani V, Atkeson T, et al. Exposure of iPSC-
804 derived human microglia to brain substrates enables the generation and manipulation of diverse
805 transcriptional states in vitro. Nat Immunol. 2023 Aug;24(8):1382–90.

806 **Main Figures**

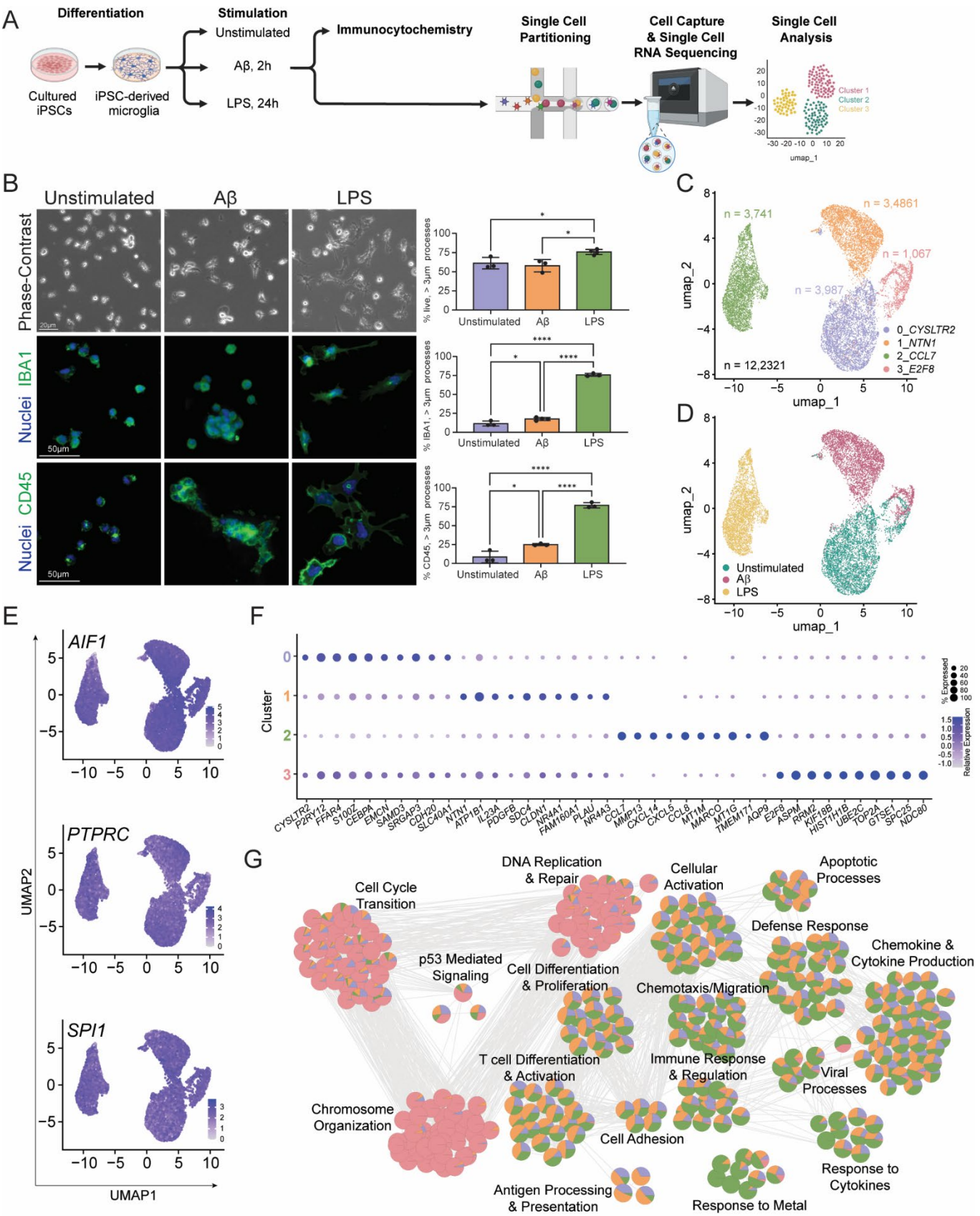

807 **Figure 1. Aβ and LPS drive distinct morphological and transcriptional activation states in**
808 **iMGLs.** (**A**) Schematic of Aβ and LPS stimulation protocol and scRNA-seq analysis pipeline. (**B**)
809 Representative phase-contrast and IBA1/CD45 immunofluorescence images showing distinct
810 morphological phenotypes in unstimulated, Aβ-treated, and LPS-treated iMGLs. Quantification of cells
811 bearing at least one process >3 μm revealed that unstimulated cells display small somas with fine
812 processes (61.21 ± 10.3%); Aβ-treated cells exhibit elongated, polarized processes with minimal
813 soma enlargement (61.06 ± 11.3%); whereas LPS-treated cells show hypertrophic morphologies
814 characterized by enlarged somas, thickened highly branched processes, and occasional granular
815 morphologies (75.92 ± 6.8%, $p < 0.05$ vs. unstimulated and Aβ). Fixed/stained cultures confirmed a
816 significant increase in process-bearing cells for Aβ ($p < 0.05$ vs. unstimulated) and highly significant
817 elevations for LPS ($p < 0.0001$ vs. unstimulated and Aβ) in both $IBA1^+$ and $CD45^+$ populations. Data
818 represent mean ± SD; significance determined by one-way ANOVA with Tukey's multiple
819 comparisons test. (**C–D**) UMAP visualization of 12,231 high-quality iMGLs by scRNA-seq, showing
820 segregation into four transcriptional clusters, largely categorized by treatment condition. (**E**)
821 Dimensional feature plots showing expression of canonical microglial identity genes (*AIF1, PTPRC,*
822 and *SPI1*) across all clusters. (**F**) Dot plot showing the top 10 differentially expressed genes for each
823 cluster. (G) Gene ontology (GO) enrichment analysis performed in Cytoscape ClueGO (v3)
824 highlighting stimulus-responsive enrichment of biological process (BP), molecular function (MF), and
825 cellular component (CC) pathways for each cluster.

826

827

828

829

830

831

832

833

834

835

836

837

838

839

840

841

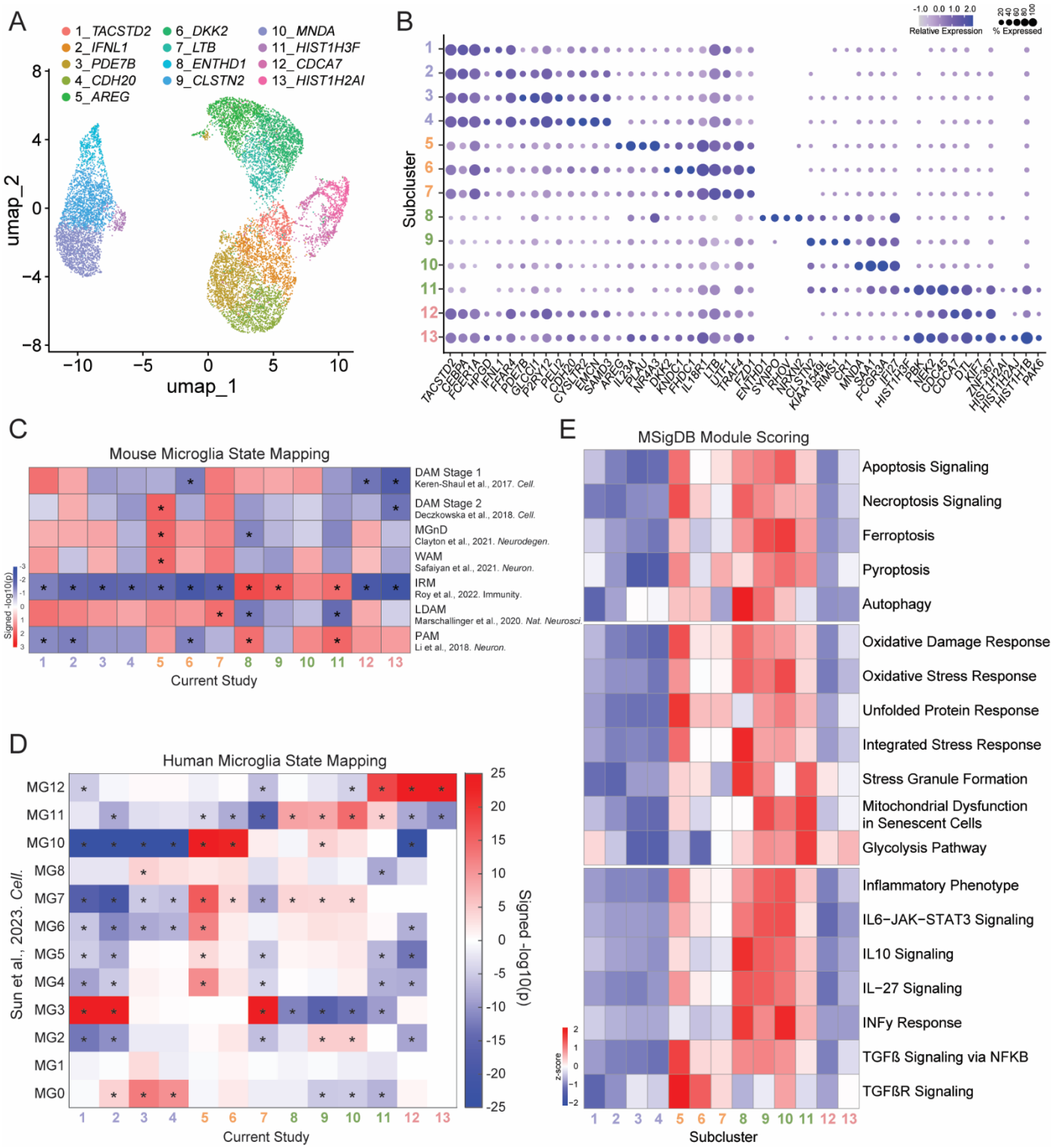

Figure 2. Subclustering Analysis reveals stimulus-specific microglial heterogeneity and links Aβ- and LPS-responsive states to in vivo microglia signatures. (**A**) UMAP visualization of subclustering results, showing 13 transcriptionally distinct microglial subclusters derived from the four major clusters identified in Figure 1. (**B**) Dot plot showing the top 4 differentially expressed genes for each subcluster. (**C**) Heatmap comparing subcluster gene sets to published rodent microglial signatures (Stage 1 and 2 Disease-associated microglia (DAM), neurodegenerative microglia

848 (MGnD), white matter-associated microglia (WAM), interferon response microglia (IRM), lipid droplet-
849 associated microglia (LDAM), and proliferative region-associated microglia (PAM). Gene set
850 enrichment analysis (GSEA) was performed on subcluster-specific ranked gene lists (log_2FC-
851 weighted – log10 adjusted *p*) and results were considered significant at adjusted $p < 0.05$. (**D**)
852 Heatmap showing enrichment of reported human AD-associated microglial states (MG0 – MG12)
853 across subclusters. GSEA was performed using the 12 microglial state signatures and the plotted
854 values represent sign (NES) x -log10(adjusted *p*) for each signature. (**E**) Module scoring was
855 performed using gene sets from the Molecular Signature Database (MSigDB) related to cell death,
856 cellular stress, and inflammatory signaling. per-cell scores were calculated s using Seurat's
857 AddModuleScore function, averaged across subclusters, and z-scored for visualization.

858

859

860

861

862

863

864

865

866

867

868

869

870

871

872

873

874

875

876

877

878

879

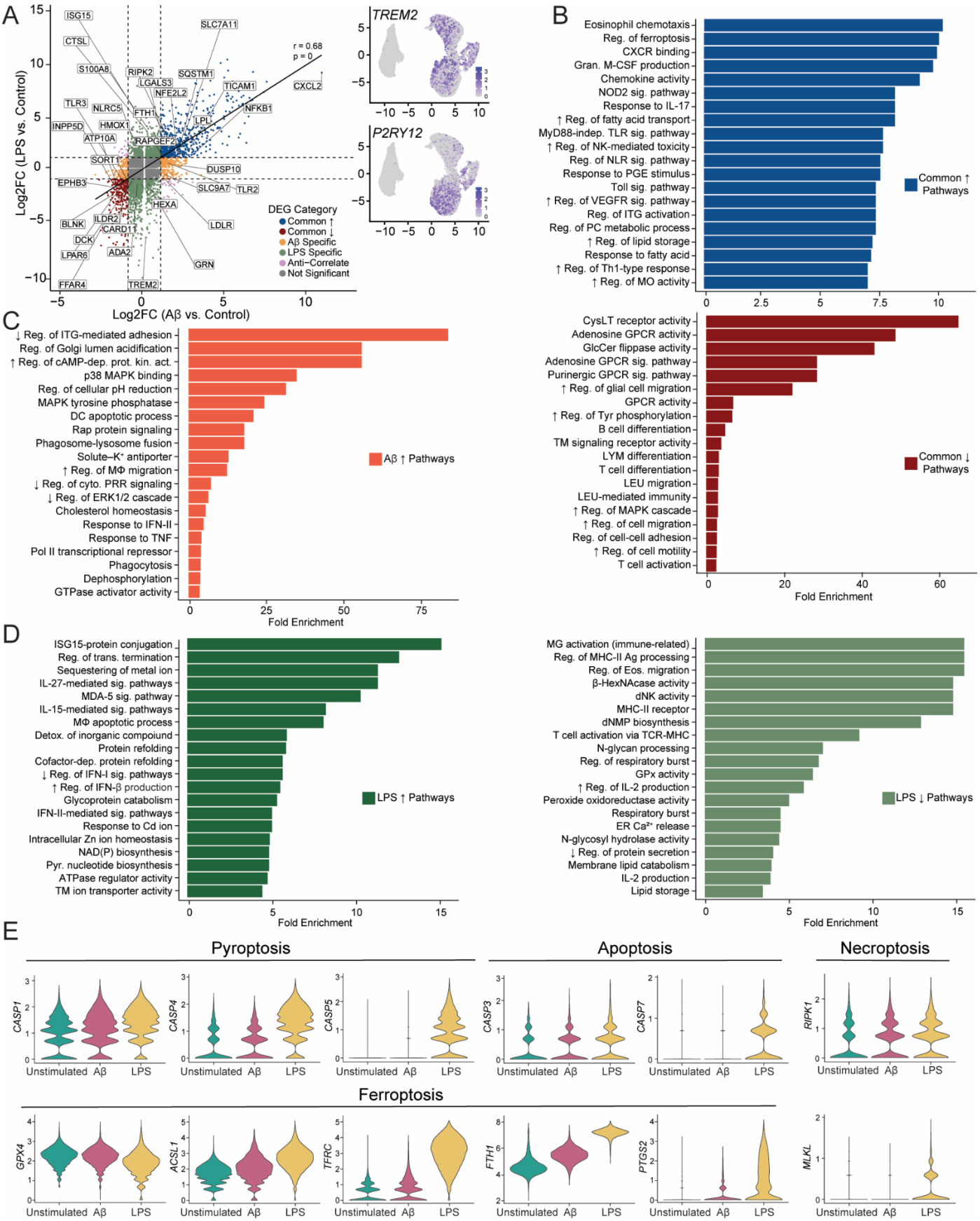
A
Log2FC (LPS vs. Control)
Log2FC (Aβ vs. Control)
r = 0.68
p = 0
ISG15
CTSL
S100A8
RIPK2
LGALS3
SQSTM1
SLC7A11
TICAM1
CXCL2
NFE2L2
TLR3
NLRC5
FTH1
NFKB1
INPP5D
HMOX1
LPL
ATP10A
RAPGEF2
SORT1
DUSP10
EPHB3
SLC9A7
TLR2
HEXA
BLNK
ILDR2
CARD11
LDLR
DCK
LPAR6
ADA2
GRN
FFAR4
TREM2
DEG Category
Common ↑
Common ↓
Aβ Specific
LPS Specific
Anti−Correlate
Not Significant
TREM2
P2RY12
B
Eosinophil chemotaxis
Reg. of ferroptosis
CXCR binding
Gran. M-CSF production
Chemokine activity
NOD2 sig. pathway
Response to IL-17
↑ Reg. of fatty acid transport
MyD88-indep. TLR sig. pathway
↑ Reg. of NK-mediated toxicity
Reg. of NLR sig. pathway
Response to PGE stimulus
Toll sig. pathway
↑ Reg. of VEGFR sig. pathway
Reg. of ITG activation
Reg. of PC metabolic process
↑ Reg. of lipid storage
Response to fatty acid
↑ Reg. of Th1-type response
↑ Reg. of MO activity
Common ↑ Pathways
CysLT receptor activity
Adenosine GPCR activity
GlcCer flippase activity
Adenosine GPCR sig. pathway
Purinergic GPCR sig. pathway
↑ Reg. of glial cell migration
GPCR activity
↑ Reg. of Tyr phosphorylation
B cell differentiation
TM signaling receptor activity
LYM differentiation
T cell differentiation
LEU migration
LEU-mediated immunity
↑ Reg. of MAPK cascade
↑ Reg. of cell migration
Reg. of cell-cell adhesion
↑ Reg. of cell motility
T cell activation
Common ↓ Pathways
Fold Enrichment
C
↓ Reg. of ITG-mediated adhesion
Reg. of Golgi lumen acidification
↑ Reg. of cAMP-dep. prot. kin. act.
p38 MAPK binding
Reg. of cellular pH reduction
MAPK tyrosine phosphatase
DC apoptotic process
Rap protein signaling
Phagosome-lysosome fusion
Solute–K⁺ antiporter
↑ Reg. of MΦ migration
↓ Reg. of cyto. PRR signaling
↓ Reg. of ERK1/2 cascade
Cholesterol homeostasis
Response to IFN-II
Response to TNF
Pol II transcriptional repressor
Phagocytosis
Dephosphorylation
GTPase activator activity
Aβ ↑ Pathways
Fold Enrichment
D
ISG15-protein conjugation
Reg. of trans. termination
Sequestering of metal ion
IL-27-mediated sig. pathways
MDA-5 sig. pathway
IL-15-mediated sig. pathways
MΦ apoptotic process
Detox. of inorganic compoiund
Protein refolding
Cofactor-dep. protein refolding
↓ Reg. of IFN-I sig. pathways
↑ Reg. of IFN-β production
Glycoprotein catabolism
IFN-II-mediated sig. pathways
Response to Cd ion
Intracellular Zn ion homeostasis
NAD(P) biosynthesis
Pyr. nucleotide biosynthesis
ATPase regulator activity
TM ion transporter activity
LPS ↑ Pathways
Fold Enrichment
MG activation (immune-related)
Reg. of MHC-II Ag processing
Reg. of Eos. migration
β-HexNAcase activity
dNK activity
MHC-II receptor
dNMP biosynthesis
T cell activation via TCR-MHC
N-glycan processing
Reg. of respiratory burst
GPx activity
↑ Reg. of IL-2 production
Peroxide oxidoreductase activity
Respiratory burst
ER Ca²⁺ release
N-glycosyl hydrolase activity
↓ Reg. of protein secretion
Membrane lipid catabolism
IL-2 production
Lipid storage
LPS ↓ Pathways
Fold Enrichment
E
Pyroptosis
Apoptosis
Necroptosis
CASP1
CASP4
CASP5
CASP3
CASP7
RIPK1
Ferroptosis
GPX4
ACSL1
TFRC
FTH1
PTGS2
MLKL
Unstimulated
Aβ
LPS

880

881 **Figure 3. Aβ and LPS induce shared and distinct transcriptional stress responses**. (**A**)
882 Differential gene expression profiles in Aβ- and LPS-treated microglia compared to unstimulated
883 controls reveal shared and stimulus-specific responses, and stimulus-responsive markers. Feature
884 plots on the right show expression of *TREM2* and *P2RY12*. (**B**) GO term enrichment of shared
885 upregulated and downregulated genes. (**C**) GO term enrichment of upregulated genes upon Aβ
886 treatment. (**D**) GO term enrichment of upregulated and downregulated genes upon LPS treatment.
887 (**E**) Violin plots showing expression of genes related to pyroptosis *(CASP1*, *CASP4*, and *CASP5*),
888 apoptosis (*CASP3* and *CASP7*), ferroptosis (*GPX4, ACSL4*, *TFRC*, *FTH1*, and *PTGS2*) and
889 necroptosis (*RIPK1, MLKL*), each of which exhibited significantly increased or decreased expression
890 in Aβ- or/and LPS-treated microglia relative to unstimulated controls (adjusted $p < 0.0001$).

891
892
893
894
895
896
897
898
899
900
901
902
903
904
905
906
907
908
909
910
911
912

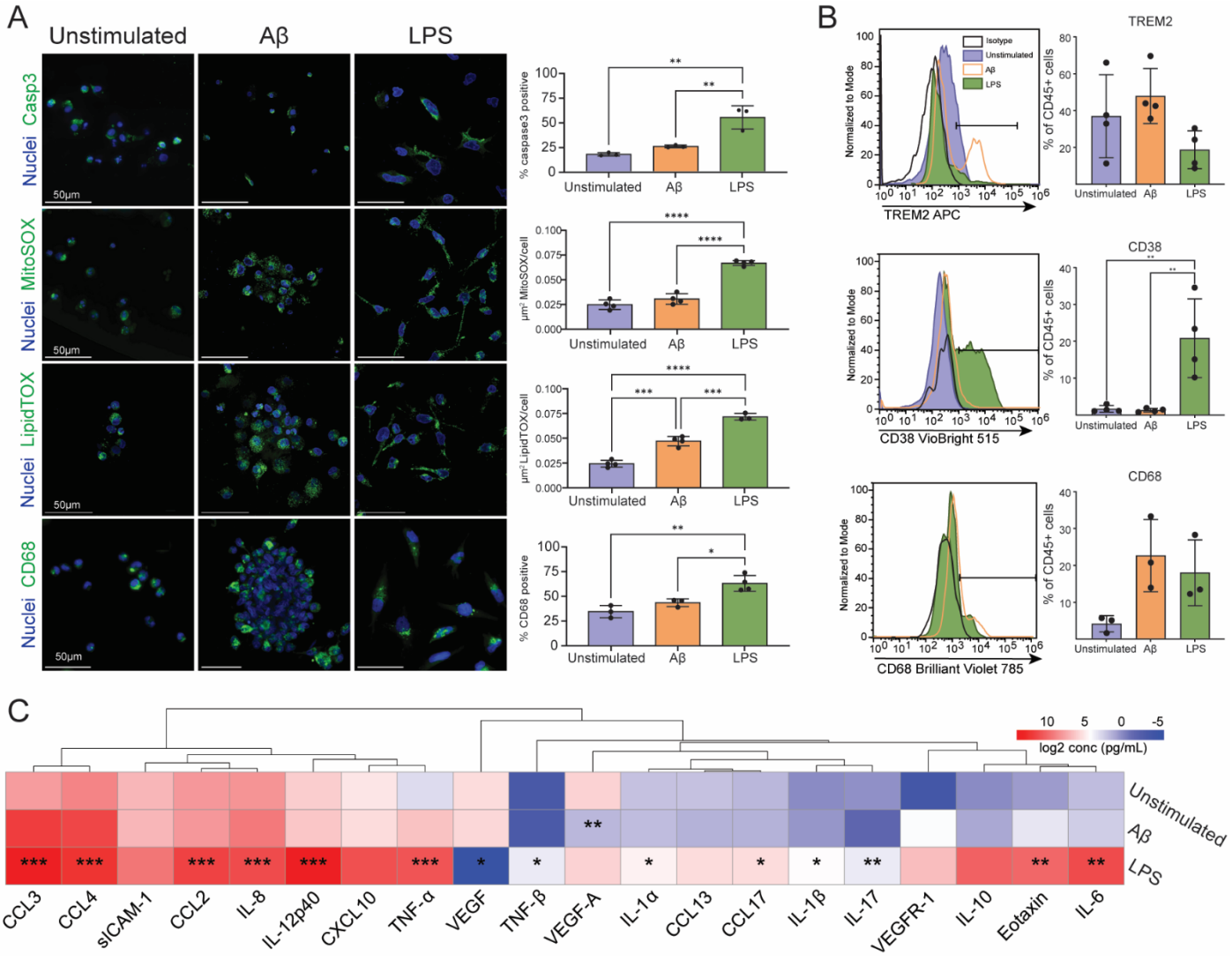

Figure 4. Cellular assays confirmed Aβ- and LPS-induced cellular stress and inflammatory responses. (**A**) Quantification of cleaved caspase-3 (positive nuclei), MitoSOX and LipidTOX (stained area normalized to nuclei count), and CD68 (positive cells) across three conditions. Data represent mean ± SD. *p < 0.05 (ANOVA with Tukey's multiple comparisons). (**B**) Flow cytometry analysis of TREM2, CD68 and CD38 expression across three conditions. Data represent mean ± SD. Significance: *p < 0.05 (ANOVA with Tukey's multiple comparisons) (**C**) Cytokine profiling reveals Aβ- and LPS-induced cytokine/chemokine responses, normalized by log2 transformation.

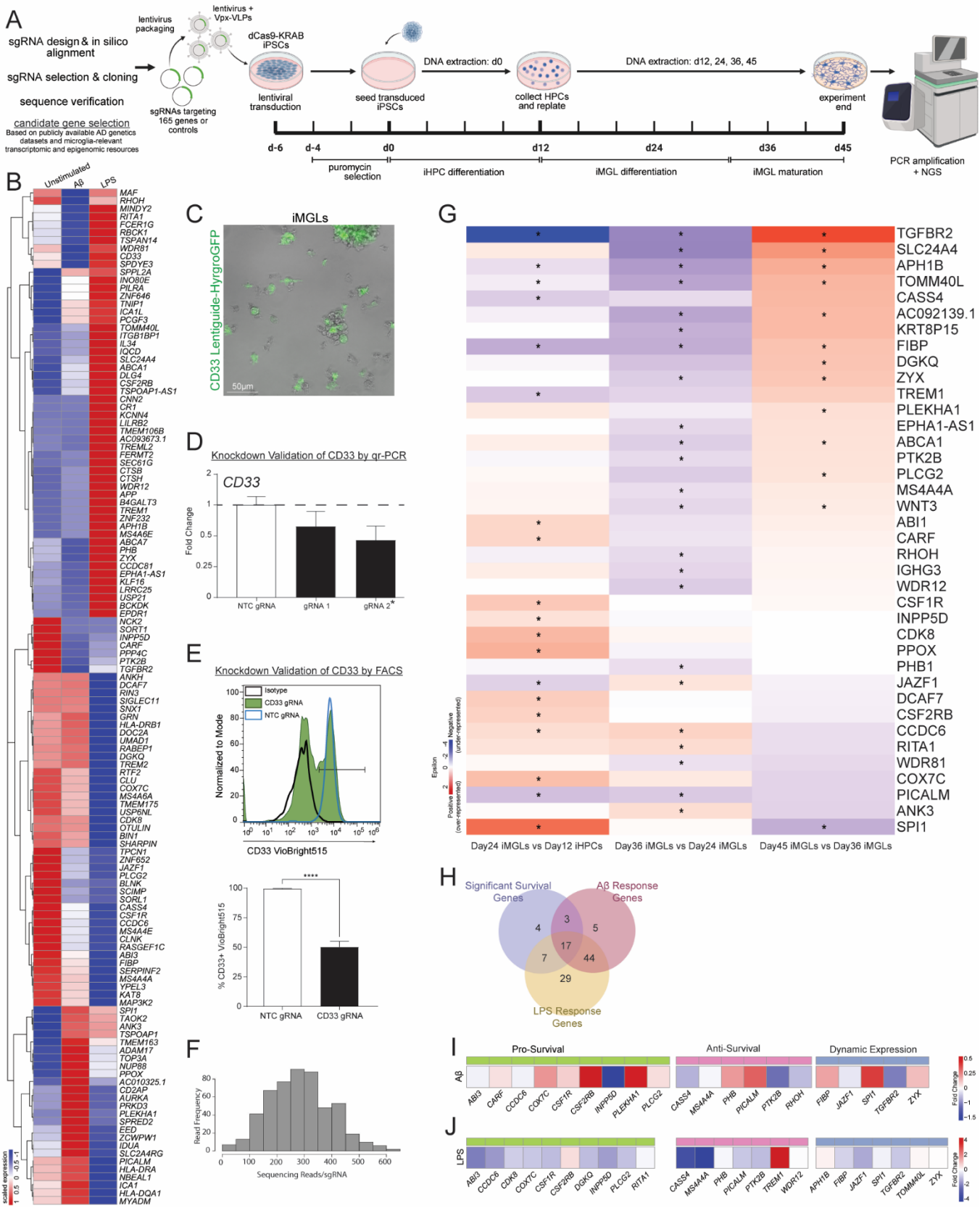
A
sgRNA design & in silico alignment
sgRNA selection & cloning
sequence verification
candidate gene selection
Based on publicly available AD genetics datasets and microglia-relevant transcriptomic and epigenomic resources
lentivirus packaging
lentivirus + Vpx-VLPs
sgRNAs targeting 165 genes or controls
dCas9-KRAB iPSCs
lentiviral transduction
seed transduced iPSCs
DNA extraction: d0
collect HPCs and replate
DNA extraction: d12, 24, 36, 45
experiment end
PCR amplification + NGS
d-6
d-4
d0
d12
d24
d36
d45
puromycin selection
iHPC differentiation
iMGL differentiation
iMGL maturation
B
Unstimulated
Aβ
LPS
scaled expression
C
iMGLs
CD33 Lentiguide-HyrgroGFP
50µm
D
Knockdown Validation of CD33 by qr-PCR
CD33
Fold Change
NTC gRNA
gRNA 1
gRNA 2*
E
Knockdown Validation of CD33 by FACS
Isotype
CD33 gRNA
NTC gRNA
Normalized to Mode
CD33 VioBright515
% CD33+ VioBright515
****
NTC gRNA
CD33 gRNA
F
Read Frequency
Sequencing Reads/sgRNA
G
TGFBR2
SLC24A4
APH1B
TOMM40L
CASS4
AC092139.1
KRT8P15
FIBP
DGKQ
ZYX
TREM1
PLEKHA1
EPHA1-AS1
ABCA1
PTK2B
PLCG2
MS4A4A
WNT3
ABI1
CARF
RHOH
IGHG3
WDR12
CSF1R
INPP5D
CDK8
PPOX
PHB1
JAZF1
DCAF7
CSF2RB
CCDC6
RITA1
WDR81
COX7C
PICALM
ANK3
SPI1
Epsilon
Negative (under-represented)
Positive (over-represented)
Day24 iMGLs vs Day12 iHPCs
Day36 iMGLs vs Day24 iMGLs
Day45 iMGLs vs Day36 iMGLs
H
Significant Survival Genes
Aβ Response Genes
LPS Response Genes
4
3
5
17
7
44
29
I
Pro-Survival
Anti-Survival
Dynamic Expression
Aβ
ABI3
CARF
CCDC6
COX7C
CSF1R
CSF2RB
INPP5D
PLEKHA1
PLCG2
CASS4
MS4A4A
PHB
PICALM
PTK2B
RHOH
FIBP
JAZF1
SPI1
TGFBR2
ZYX
Fold Change
J
LPS
ABI3
CCDC6
CDK8
COX7C
CSF1R
CSF2RB
DGKQ
INPP5D
PLCG2
RITA1
CASS4
MS4A4A
PHB
PICALM
PTK2B
TREM1
WDR12
APH1B
FIBP
JAZF1
SPI1
TGFBR2
TOMM40L
ZYX
Fold Change

926

927 **Figure 5. CRISPRi functional screening reveals partial overlap between AD-risk genes and**
928 **microglial stress response genes**. (**A**) Schematic of the CRISPRi screen targeting 168 AD-
929 associated microglia genes. (**B**) Expression analysis identified 127 genes expressed in iMGLs across
930 three conditions, showing distinct expression patterns. (**C**) Representative image of iMGLs infected
931 with lentiviral sgRNA targeting CD33 at day 40 (10 days post-infection). (**D-E**) Knockdown validation
932 of CD33 by qRT-PCR (fold-change expression) and flow cytometry (mean ± SD; significant by
933 Welch's t-test, $p < 0.0001$). (**F**) sgRNA distribution in iPSCs infected with the pooled lentiviral library
934 targeting 168 AD-associated microglia genes. (**G**) Survival screen identifies 31 genes regulating iMGL
935 survival that were also expressed in scRNA-seq data; these genes were categorized as pro-survival,
936 anti-survival, or dynamic regulators. (**H**) Venn diagram showing 27 genes overlapping between
937 survival hits and 127 DEGs induced by Aβ or LPS; 17 genes were shared across Aβ-responsive,
938 LPS-responsive, and survival-linked categories. (**I-J**) Heatmap showing fold changes in gene
939 expression relative to unstimulated controls under Aβ or LPS stimulation, grouped by pro-survival,
940 anti-survival, or dynamic regulators.

Supplementary Figures

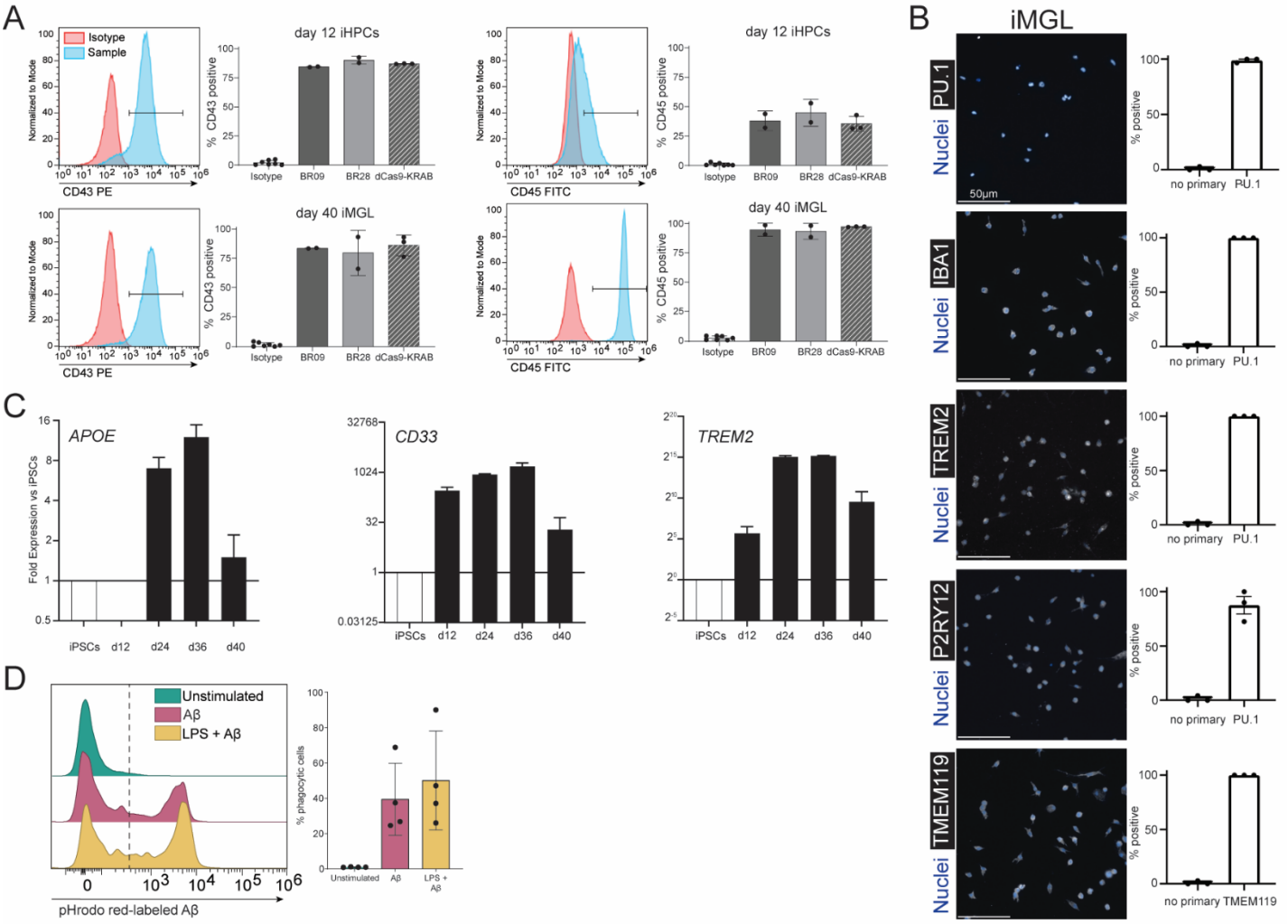

Supplementary Figure 1. Benchmarking iMGL differentiation of dCas9-KRAB iPSC line against control ROSMAP iPSC lines. (**A**) Flow cytometry analysis of CD43 and CD45 expression at day 12 and day 40 of differentiation across three iPSC lines. Representative histograms and quantification illustrate robust expression of myeloid markers during iMGL differentiation. (**B**) Immunocytochemistry (ICC) images and corresponding quantification showing dCas9-KRAB iPSC-derived iMGLs express canonical microglial markers including PU.1, IBA1, TREM2, P2RY12, and TMEM119. (**C**) Quantitative RT-PCR analysis of APOE, CD33, and TREM2 expression across multiple differentiation stages, demonstrating transcriptional maturation of iMGLs. (**D**) Phagocytosis assay showing dCas9-KRAB iPSC-derived iMGLs respond to Aβ stimulation, with enhanced phagocytic uptake upon LPS or cytokine treatment, as evidenced by flow cytometry and quantification.

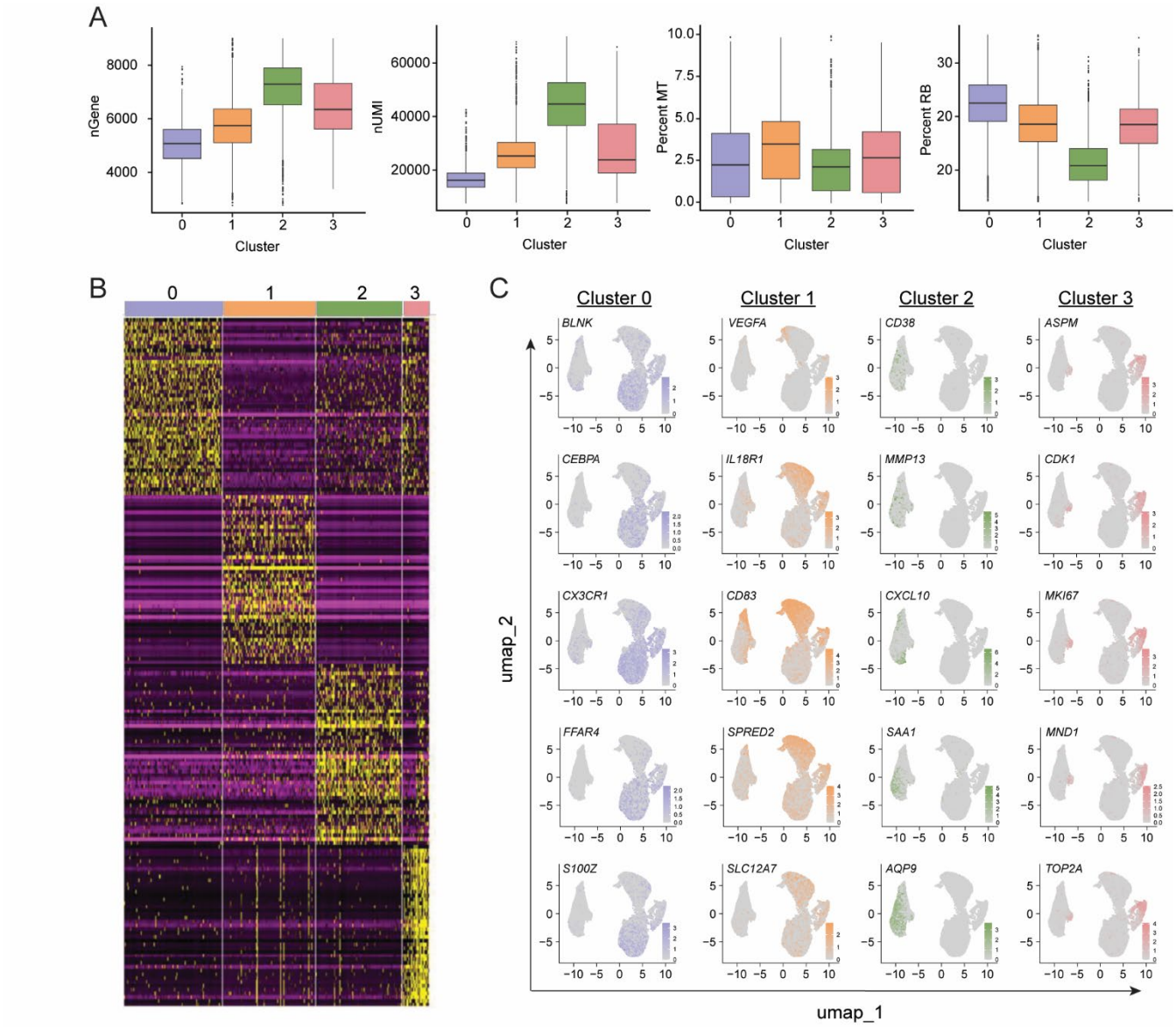

954 **Supplementary Figure 2. Single-cell RNA-seq quality control and microglial marker gene**
955 **expression.** (**A**) Boxplots showing quality control metrics across individual clusters, including number
956 of detected genes (nGene), number of UMIs (nUMI), percentage of mitochondrial reads (percent.mt),
957 and percentage of ribosomal reads (percent.RB). (**B**) Heatmap displaying the top 50 differentially
958 expressed genes defining each cluster. (**C**) Feature plots illustrating the expression of microglial
959 marker genes across clusters.

960

961

962

963

964 **Supplementary Tables**

965 **Table S1**. Media and Assay Reagents

966 **Table S2**. iMGL Markers by Cluster and ClueGO Pathways

967 **Table S3**. iMGL Markers by Subcluster and MSigDB Gene Sets

968 **Table S4**. Stimulus Specific DEGs and GO Terms

969 **Table S5**. MesoScale Cytokine Concentrations

970 **Table S6**. Candidate Survival Genes from CRISPRi Screens